AMEGHINIANA
A GONDWANAN PALEONTOLOGICAL JOURNAL

RICH AND SPECIALIZED PLANT-INSECT ASSOCIATIONS IN A MIDDLE–LATE PALEOCENE (58–60 MA) NEOTROPICAL RAINFOREST (BOGOTÁ FORMATION, COLOMBIA)

L. ALEJANDRO GIRALDO[1,2]
CONRAD LABANDEIRA[3,4,5]
FABIANY HERRERA[6]
MÓNICA CARVALHO[2,7]

[1]Programa de Biología, Departamento de Ciencias Biológicas, Universidad EAFIT, 050022 Medellín, Colombia.
[2]Smithsonian Tropical Research Institute, Box 0843-03092, Ancón, Panamá, Panamá.
[3]Department of Paleobiology, National Museum of Natural History, Smithsonian Institution, 20013 Washington, DC, USA.
[4]Department of Entomology and Behavior, Ecology, Evolution, and Systematics Program, University of Maryland, 20742 College Park, USA.
[5]School of Life Sciences, Capital Normal University, 100048 Beijing, China.
[6]Chicago Botanic Garden, 60022 Chicago, Illinois, USA.
[7]Grupo de Investigación Paleontología Neotropical Tradicional y Molecular (PaleoNeo), Facultad de Ciencias Naturales y Matemáticas, Universidad del Rosario, 111711 Bogotá, Colombia.

Submitted: August 26th, 2020 - **Accepted:** February 17th, 2021 - **Published:** April 30th, 2021

To cite this article: L. Alejandro Giraldo, Conrad Labandeira, Fabiany Herrera, & Mónica Carvalho (2021). Rich and specialized plant-insect associations in a middle–late Paleocene (58–60 Ma) Neotropical rainforest (Bogotá Formation, Colombia). *Ameghiniana 58*(2), 75–99.

To link to this article: http://dx.doi.org/10.5710/AMGH.17.02.2021.3390

PLANT PREDATION FROM PALEOCENE NEOTROPICAL RAINFORESTS

Plant-insect associations in leaf fossils from the Bogotá Formation, central Colombia, indicate much more intense herbivory than elsewhere.

FIRST FOSSIL RECORD OF SAWSHARKS FROM CHILE

The genus *Pliotrema* is described from the Miocene–Pliocene Bahía Inglesa Formation, Atacama region.

NEW ERYTHROSUCHID ARCHOSAURIFORM FROM INDIA

The new genus and species *Bharitalasuchus tapani* is described from the Triassic Yerrapalli Formation.

AMEGHINIANA - 2021 - Volume 58 (2): 75–99 ARTICLES

ISSN 0002-7014

RICH AND SPECIALIZED PLANT-INSECT ASSOCIATIONS IN A MIDDLE–LATE PALEOCENE (58–60 MA) NEOTROPICAL RAINFOREST (BOGOTÁ FORMATION, COLOMBIA)

L. ALEJANDRO GIRALDO[1,2], CONRAD LABANDEIRA[3,4,5], FABIANY HERRERA[6], AND MÓNICA CARVALHO[2,7]

[1]Programa de Biología, Departamento de Ciencias Biológicas, Universidad EAFIT, 050022 Medellín, Colombia. *lgiral71@eafit.edu.co*

[2]Smithsonian Tropical Research Institute, Box 0843-03092, Ancón, Panamá, Panamá. *carvalhom@si.edu*

[3]Department of Paleobiology, National Museum of Natural History, Smithsonian Institution, 20013 Washington, DC, USA. *labandec@si.edu*

[4]Department of Entomology and Behavior, Ecology, Evolution, and Systematics Program, University of Maryland, 20742 College Park, USA.

[5]School of Life Sciences, Capital Normal University, 100048 Beijing, China.

[6]Chicago Botanic Garden, 60022 Chicago, Illinois, USA. *fherrera@chicagobotanic.org*

[7]Grupo de Investigación Paleontología Neotropical Tradicional y Molecular (PaleoNeo), Facultad de Ciencias Naturales y Matemáticas, Universidad del Rosario, 111711 Bogotá, Colombia.

Abstract. Plant predation by insects is a major driver of high plant diversity in modern tropical forests. Previous reports of leaf damage in middle–late Paleocene Neotropical rainforests of Cerrejón, Colombia, show that leaf herbivory was abundant but of low diversity, mainly inflicted by generalized feeders. Here, we present and describe plant-insect associations in leaf fossils from the middle–late Paleocene Bogotá Formation, central Colombia, to test whether the high abundance and low richness of insect damage typified early evolving Neotropical rainforests. The Bogotá flora records the highest richness and frequency of insect-damage associations among comparable Paleocene floras in North America, Patagonia, and Europe, as well as the highest number of leaf mines and galling associations. These results indicate that by the middle–late Paleocene, plant-insect herbivore interactions were much more intense and host-specialized in Neotropical rainforests of the Bogotá region than elsewhere. The rich and frequent galling associations, a distinctive feature of the Bogotá flora, are consistent with the preferential use of canopy leaves by galling insects seen in modern Neotropical rainforests. Our results also indicate differences in plant-insect associations among Paleocene Neotropical rainforests, perhaps reflecting a geographically heterogeneous ecological recovery from the end-Cretaceous ecological crisis. Plant insect-associations in the Bogotá flora also suggest a deep historical context for negative density-dependence as a potential driver (and maintainer) of the high plant diversity observed in modern Neotropical rainforests.

Key words. Fossil leaves. Neotropics. Herbivory. Negative density-dependence. Host-specialized interactions. Leaf damage. Paleobotany.

Resumen. ALTA RIQUEZA Y ESPECIALIZACIÓN DE ASOCIACIONES PLANTA-INSECTO EN UN BOSQUE LLUVIOSO NEOTROPICAL DEL PALEOCENO MEDIO-TARDÍO (58–60 MA) (FORMACIÓN BOGOTÁ, COLOMBIA)**.** El consumo de plantas por insectos impulsa la alta diversidad de plantas de los bosques lluviosos tropicales modernos. Reportes de daños en hojas de los bosques lluviosos Neotropicales del Paleoceno medio-tardío de Cerrejón, Colombia, indican una abundante pero poco diversa herbivoría foliar, principalmente infligida por herbívoros generalistas. En este estudio, presentamos y describimos asociaciones planta-insecto en hojas fósiles de la Formación Bogotá (Paleoceno medio-tardío), centro de Colombia, para probar si la alta abundancia y baja riqueza de daños de insectos tipificaron la evolución temprana de los bosques lluviosos Neotropicales. La flora de Bogotá registra la mayor riqueza y frecuencia de asociaciones planta-insecto entre floras comparables del Paleoceno en América del Norte, Patagonia y Europa, además del mayor número de minas y agallas. Estos resultados indican que, para el Paleoceno medio–tardío, las interacciones planta-insecto herbívoro eran mucho más intensas y especializadas en los bosques lluviosos Neotropicales de Bogotá que en otros lugares. La alta riqueza y frecuencia de agallas, una característica distintiva de la flora de Bogotá, coincide con observaciones en bosques lluviosos Neotropicales modernos donde los insectos generadores de agallas usan preferentemente hojas del dosel. Nuestros resultados indican diferencias en las asociaciones planta-insecto entre los bosques lluviosos Neotropicales del Paleoceno, quizás reflejando una recuperación ecológica geográficamente heterogénea tras la crisis ecológica del final del Cretácico. Las asociaciones planta-insecto en la flora de Bogotá sugieren un profundo contexto histórico de la denso-dependencia negativa como potencial impulsor (y mantenedor) de la alta diversidad de plantas observada en bosques lluviosos Neotropicales modernos.

Palabras clave. Hojas fósiles. Neotrópico. Herbivoría. Denso-dependencia negativa. Interacciones especializadas. Daños foliares. Paleobotánica.

PLANT PREDATION BY INSECTS is considered a driving force for high plant diversity in tropical rainforests (Janzen, 1970; Connell, 1971). Natural enemies, such as herbivores, reduce population growth rates of plant species that become locally common (Janzen, 1970; Connell, 1971), prompting plant species coexistence through negative density-depen-

dent interactions (Forrister *et al.*, 2019). This mechanism explains the strong correlation observed between the diversity of plant hosts and insect herbivores in modern ecosystems, particularly in the tropics (Novotny *et al.*, 2006, 2007; Dyer *et al.*, 2007). It also predicts similar trends in plant-insect diversity to occur over geologic time.

The bitrophic interaction between producers (plants) and their consumers (insect herbivores) can be directly assessed through well-preserved tissue damage found on fossil plant organs, commonly on leaves (*e.g.*, Labandeira *et al.*, 2007; Wilf, 2008). These insect-mediated damage traces can be quantified using a standardized system of functional feeding group (**FFG**) and damage type (**DT**) occurrences (Labandeira *et al.*, 2007) that allows plant-insect interactions to be described in a coarse- and fine grained manner, and compared across fossil floras and throughout geologic time (Wilf & Labandeira, 1999; Labandeira *et al.*, 2002a, 2002b; Wilf *et al.*, 2006). Each DT is a distinctive style of biological damage on a leaf—caused by an insect, mite, pathogen, or rarely by a myriapod or gastropod—and is defined by macromorphological features such as size, shape, occurrence, position on a leaf, and membership in a particular FFG, as well as micromorphological features such as callus tissue development, patterns of frass accumulation, and scar and egg placement in oviposition lesions (Labandeira *et al.*, 2007). In turn, FFGs are a more encompassing category of insect feeding strategies, each of which consists of similar DTs, defined by a particular mode of tissue consumption by arthropods and mostly associated with mouthpart structure (Labandeira, 2019). Pathogens, represented by viruses, bacteria and especially fungi, have a very different mode of accessing live plant tissues (Labandeira & Prevec, 2014), and are a group of DTs encompassed by a separate FFG. For leaf damage, endophytic feeding such as miners and gallers tend to reflect host-specific associations, in which a single insect species makes a distinctive DT on a specific host species at a site (Crespi *et al.*, 1997; Bairstow *et al.*, 2010). External-feeding, involving mostly leaf-chewing, typically is less specific, although the numbers of external feeding DTs have been shown to reflect the richness of damage makers in modern forests (Carvalho *et al.*, 2014). These associations between insect-feeding DTs and damage makers indicate that the association between plants and herbivorous insects in past ecosystems is potentially addressable (Wilf, 2008).

Neotropical rainforests contain an outstanding richness of plants and associated insect herbivores, yet little is known about the origin of this diversity. The plant fossil record shows that the assembly of modern Neotropical rainforests—as identified by their shared climate, leaf physiognomy, plant family composition, and canopy structure (Burnham & Johnson, 2004)—dates back to the Paleocene and was prompted by the end-Cretaceous extinction (Wing *et al.*, 2009; Graham *et al.*, 2019; Carvalho *et al.,* unpublished). Along with the middle–late Paleocene Cerrejón flora (58–60 Ma; Wing *et al.*, 2009), the localities of the Bogotá flora from central Colombia (58–60 Ma) are the earliest known examples of Neotropical rainforests (Herrera *et al.*, 2011, 2019). They provide a unique insight into plant-insect associations at the early stages in the evolution of Neotropical rainforests and allow for the testing of diversity patterns. At Cerrejón, leaf herbivory was abundant but of low diversity, mainly inflicted by generalized feeders (Wing *et al.*, 2009). This observation contrasts with modern Neotropical rainforests, where herbivore pressure is high (Coley & Aide, 1991), and insect-feeding associations are commonly rich and specialized (Dyer *et al.*, 2007).

In contrast to the coastal-floodplain and deltaic environments of the Cerrejón Formation (Jaramillo *et al.*, 2007), the Bogotá flora was deposited in lowland fluvial environments (Bayona *et al.*, 2008, 2010). This flora shares paleoclimatic, physiognomic, floristic, and ecological similarities with modern-day Neotropical rainforests, and consequently, with the Cerrejón flora (Wing *et al.*, 2009; Herrera *et al.*, 2011, 2019; Carvalho *et al.*, unpublished). Most taxa are known to belong to lineages commonly found in the lowland Neotropics, including Fabaceae (bean family) (Herrera *et al.*, 2019), Menispermaceae (moonseeds) (Herrera *et al.*, 2011), Malvaceae (mallows), Ulmaceae (elms) (Herrera *et al.*, 2014), Icacinaceae (false yams and relatives) (Stull *et al.*, 2012), as well as Annonaceae (custard apples), Araceae (aroids), Arecaceae (palms), Elaeocarpaceae, Euphorbiaceae (spurges), Lauraceae (laurels), Rhamnaceae (buckthorns), Salicaceae (willows) and Theaceae (camellias). Furthermore, the relative abundance of plant families in this flora is similar to the Cerrejón flora and to modern Neotropical rainforests.

Here, we present and describe the leaf damage of the middle–late Paleocene Bogotá flora, providing a baseline on

plant-insect associations at the early stages of Neotropical rainforest evolution. We ask whether the low diversity of insect-feeding damage observed at Cerrejón is a consistent pattern throughout middle–late Paleocene Neotropical rainforests. We also compare insect-damage frequency and diversity with temperate Paleocene floras. Insect-feeding damage in the Bogotá flora has the highest DT frequency and richness across comparable Paleocene floras. In contrast to insect-feeding damage of Cerrejón, there is also a high incidence of specialized interactions such as mines and galls. We argue that patterns of ecological recovery from the end-Cretaceous ecological crisis (Wing *et al.*, 2009) differed across early evolving Neotropical rainforests.

MATERIALS AND METHODS

Geological setting

The Bogotá Formation consists of extensive, thick siltstones, claystones, paleosols, interbedded sandstones, and sporadic conglomerates and breccias (Morón *et al.*, 2013) that crop out along the Eastern Cordillera, in central Colombia. The 1.6 km-thick depositional sequence of the Bogotá Formation is part of the Bogotá Basin and is considered to have accumulated throughout the middle–late Paleocene and early Eocene in fluvial, lowland environments that pre-date the Andean uplift in northern South America (Bayona *et al.*, 2008, 2010). A diverse array of plant and vertebrate fossils are known from these fluvial deposits, including xenungulate mammals (Villaroel, 1987), marsupials, mesoeucrocodylians, anurans, dipnoan fishes (Bloch *et al.*, 2008), turtles (Cadena, 2014), as well as squamates such as iguanians and snakes (Head *et al.*, 2012). Pollen assemblages retrieved from fossiliferous sites (Checua and Cogua; see below) belong to the T-03b-*Foveotricolpites perforates* zone of Jaramillo *et al.* (2011), indicating a middle to late Paleocene age (*c.* 60–58 Ma). Laser Ablation Inductively Coupled Plasma Mass Spectrometry (**LA-ICP-MS**) $^{206}Pb/^{238}U$ analyses on volcanic zircons retrieved from the type section of the Bogotá Formation yielded a late Paleocene age of 56.2±1.6 Ma (Bayona *et al.*, 2010).

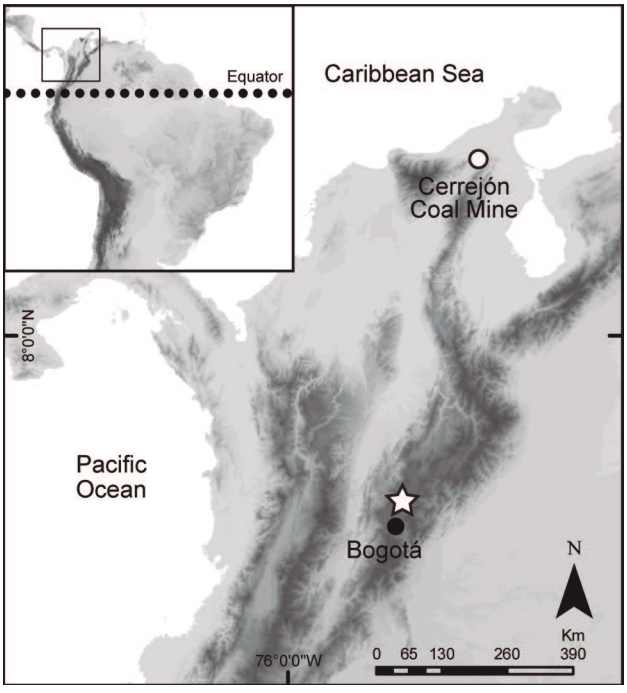

Figure 1. Collection site for leaves of the Bogotá Formation (Chechua and Cogua localities) in Cundinamarca, Colombia, indicated by a star. White circle indicates collection site for leaves of the Cerrejón Formation.

Study area

The fossil leaves come from fine-grained sandstones and siltstones collected from the Checua plant locality (5° 4′ 16.968″ N; 73° 57′ 7.92″ W), consisting of 461 fossil leaves, and the Cogua locality (5° 4′ 36.3″ N; 73° 57′ 19.08″ W), consisting of 494 fossil leaves, occurring in the municipalities of Nemocón and Cogua, respectively, in the Cundinamarca Department, Colombia (Fig. 1). The extensive mining of siltstone deposits of the Bogotá Formation in these areas provided access to largely exposed outcrops. Eleven quarries excavated at the Checua locality and four quarries excavated at the Cogua locality represent lateral variation of leaf beds within a few stratigraphic meters from each other.

Fossil leaves morphotyping and damage type scoring

We examined 955 complete to nearly complete leaf impressions (894 non-monocot angiosperms, 45 monocots, 16 ferns) from the Bogotá Formation. The leaves were classified into 56 discrete morphotypes (48 non-monocot angiosperms, six monocots, two ferns) based on leaf architecture (Ellis *et al.*, 2009). Each morphotype was provided with a unique identification number under the acronym **BF** (Bogotá Flora). Each leaf was thoroughly inspected for insect-mediated damage and evaluated for consistent and stereotypical DTs, described in Labandeira *et al.* (2007; and subsequent updates). DTs were scored for each leaf. These

DTs were then categorized by the functional feeding groups of external feeding, which encompasses hole feeding, margin feeding, skeletonization and surface feeding, and the internally feeding piercing-and-sucking, galling, mining and oviposition, and pathogen damage.

Plant-host specificity for each DT was assessed. The damage was assigned a number based on a generalization to specialization scale that was given a host-plant specificity number (or **HS** index), where 1 is generalized damage, 2 refers to damage of intermediate specificity, and 3 is specialized damage (Labandeira *et al.*, 2007). A DT found on unrelated or very distantly related plant-host morphotypes is given a designation of 1 (generalized); a DT present on more closely related morphotypes such as multiple unrelated genera within a family is provided a 2 (intermediate specificity); and a DT occurring only on one or alternatively very closely-related morphotypes is given a 3 (specialized). These categorizations correspond to polyphagy, oligophagy and monophagy, respectively, in the entomological literature.

Representative DTs were photographed using a Canon EOS 5DS R camera. Poorly preserved DTs were drawn under a camera-lucida on a Nikon SMZ1500 stereoscope. Reversible image adjustments such as white balance, temperature, and contrast were made using Adobe Photoshop CC 2018. When required, length and width measurements of DTs were made using *ImageJ* v1.51.j8 (Schneider *et al.*, 2012). Each specimen was provided with a unique identification number following the prefix **STRI**. A complete catalog of specimens, plant morphotypes and DT occurrence data used in this study, and detailed description of seven new DTs are included in the Supplementary Online Information. Further details on samples and localities can be accessed through the Geologic Sample Database of the Smithsonian Tropical Research Institute (Jaramillo, 2020). All specimens are deposited at the paleontological collections of the Museo Geológico Nacional José Royo y Gómez of the Servicio Geológico Colombiano (Colombian Geological Survey) in Bogotá, Colombia; and the Centro de Museos de la Universidad de Caldas in Manizales, Colombia.

We compared DT richness and the frequency of damaged leaves in the Bogotá flora with leaf damage quantified in other Paleocene assemblages, including the Cerrejón flora from the Ranchería Basin (Wing *et al.*, 2009). For the Western Interior of North America, we included a set of localities from several basins which form a composite regional data set, spanning from the early Danian (66 Ma) to the mid Thanetian (57 Ma); namely, Pyramid Butte, Mexican Hat, Castle Rock, Kevin's Jerky, Haz-Mat, *Persites* Paradise, Lur'd Leaves and Clarkforkian (Wilf & Labandeira, 1999; Labandeira *et al.*, 2002a, 2002b; Wilf *et al.*, 2006). European Paleocene floras included the Selandian (60–61 Ma) Menat locality, from the Menat Basin in France (Wappler *et al.*, 2009) and the middle Paleocene (58–61? Ma) Firkanten flora from Spitsbergen, Norway (Wappler & Denk, 2011). The Patagonian data set included early Danian floras (62.22–65.58 Ma) from the San Jorge Basin, namely Palacio de los Loros 1, Palacio de los Loros 2 and Las Flores localities (Donovan *et al.*, 2016, 2018). Only non-monocot angiosperm leaves, and DTs from the seven herbivory-related FFGs (hole feeding, margin feeding, skeletonization, surface feeding, piercing-and-sucking, galling and mining) were considered for consistency with previous studies. Four-hundred leaves were randomly sampled without replacement. The numbers of unique DTs (DT richness) and percentage of damaged leaves (DT frequency) were estimated from the means of 5000 iterations. For the most abundant morphotypes that recorded a high frequency of galling DTs (five plant hosts with >20 specimens and more than 20% of their leaves damaged with galls), we resampled 20 leaves at 5000 iterations in order to assess insect-damage frequency and richness on individual plant hosts. Reported uncertainties are ±1*s*.

To assess whether the preservation quality seen in the Bogotá flora could affect DT richness, we conducted a parallel set of analyses using a conservative scoring to DTs that were likely to be misidentified in comparable floras due to taphonomy (*e.g.*, leaf transport, preservation in coarser sediments, leaf coalification). These include several piercing-and-sucking and galling DTs identified based on detailed internal features that would potentially be lost if found in coarse sediments or in coalified leaves (see Supplementary Online Information, Supplementary Table 1). The percentage of damaged leaves and DT richness were quantified as described above for comparison (Supplementary Online Information, Supplementary Figure 1). The conservative scoring database is also provided in the Supplementary Online Information. All analyses were conducted with R version 4.0 (R Core Team, 2020).

DAMAGE TYPES DESCRIPTIONS

Nine FFGs were present in the Bogotá flora: hole feeding, margin feeding, skeletonization, surface feeding, piercing-and-sucking, mining, galling, oviposition, and pathogens. Eighty-six insect-mediated (80 of which are related to insect-feeding and six to oviposition) and four pathogen DTs were found in the Bogotá flora. This represents an elevated insect damage spectrum of FFGs and DTs, previously unrecorded in the fossil record.

Ten hole feeding DTs were documented and are illustrated in Figure 2. Circular and ellipsoidal holes measure 0.1–10.9 mm in diameter (DT1, DT2, DT4; Fig. 2.1–2.2) and polylobate holes range between 1.1–24.1 mm in length by 0.4–8.4 mm in width (DT3, DT5; Fig. 2.3–2.5). A series of elliptical to triangular holes positioned at the intersections of primary and secondary veins (DT57; Fig. 2.6) measure 1.2–6.5 mm in length by 0.6–5.1 mm in width. Curvilinear to rectilinear elongate holes (DT7; Fig. 2.7–2.8) measure 1.5–10.4 mm in length by 0.3–2.9 mm in width. Clustered comma-shaped or elliptical holes scattered along a leaf margin (DT9; Fig. 2.9) measure 1.2–7.8 mm in length by 0.6–1.4 mm in width. More or less symmetrical perforations occurring on either side of a midvein (DT63; Fig. 2.10) measure 1.4–5.3 mm in length by 1.0–4.7 mm in width. Curvilinear to rectilinear elongate holes with parallel sides and length-to-width ratios greater than 2.5 (DT8; Fig. 2.11) measure 1.3–4.5 mm in length by 0.5–2.5 mm in width. Reaction rims surrounding any of the aforementioned hole feeding traces measure 0.1–0.2 mm in width.

Six margin feeding DTs (Fig. 3.1–3.6) include semicircular, shallow excisions along the leaf margin (DT12; Fig. 3.1) that measure 1.5–20.4 mm in width and are 0.9–15.1 mm deep, and excisions removing the leaf apex (DT13, Fig. 3.2) that are 0.5–27.6 mm deep. Margin feeding traces that reach the midvein (DT14; Fig. 3.3) measure 1.0–27.6 mm in width and are 0.5–78.8 mm deep. Excisions that expand towards the midvein (DT15; Fig. 3.4) measure 2.5–44.8 mm in width and are 3.2–27.6 mm deep, and trenched excisions with width expansions and constrictions towards a primary vein (DT198; Fig. 3.5) measure 4.5 mm in width and are 4.4 mm deep. The extensive removal of up to 75% of the leaf lamina (DT395; Fig. 3.6) was observed in two leaf samples. Reaction rims associated with margin feeding traces are 0.1–0.2 mm thick.

Five skeletonization DTs were observed and are illustrated in Figure 3. Irregularly shaped skeletonization patches with poorly developed or entirely lacking reaction rims (DT16; Fig. 3.7) range 2.1–25.1 mm in length by 1.4–16.1 mm in width, and those with thick reaction rims (DT17; Fig. 3.8) measure 4.3–28.8 mm in length by 3.0–8.1 mm in width. Curvilinear patches of skeletonized tissue (DT20; Fig. 3.9) measure 4.6–10.5 mm in length by 0.8–1.2 mm in width, and extensive skeletonization occurring at a leaf base (DT56; Fig. 3.10) measure 28.6 mm in length by 27.4 mm in width. Skeletonization along the leaf margin characterized by the removal the of the finest veins (DT21; Fig. 3.12–3.13) measure 4.2–20.1 mm in length by 2.8–13.9 mm in width. Reaction rims, when present, associated with skeletonization measure 0.1 mm in width.

Surface feeding damage includes 10 DTs illustrated in Figure 4. Linear surface abrasions along major veins (DT25; Fig. 4.1, dotted lines) measure 5.3–10.9 mm in length by 0.3–0.8 mm in width. Polylobate surface abrasions with poorly developed, or entirely lacking reaction rims (DT29; Fig. 4.2) range 0.7–2.1 mm in length by 0.6–1.4 mm in width, and polylobate surface abrasions with distinct reaction rims (DT30; Fig. 4.1, white arrow) measure 0.7–2.4 mm in length by 0.7–1.4 mm in width. Circular to elliptical surface abrasions with distinct reaction rims (DT31; Fig. 4.3) measure 0.6–1.4 mm in diameter. Elongate surface abrasions with a thick reaction tissue that extends into the abraded area as a wedge-like structure (DT203; Fig. 4.4–4.5) measure 1.7–3 mm in length by 0.3–1.1 mm in width. Elongate surface abrasions with length-to-width ratios of 6.1 occurring along the leaf margin (DT155; Fig. 4.6–4.7) measure up to 18.9 mm in length by 1.4–6.5 mm in width. Parallel-sided slots with a thick reaction rim, adjacent and parallel to major veins (DT317; Fig. 4.8), measure 0.6–1.4 mm in length by 0.4–1.0 mm in width. Irregular surface abrasions that occur along the leaf margin and have wedge-like extensions towards the inner abraded area (DT365; Fig. 4.9–4.10) measure 11.8 mm in length by 0.1–0.4 mm in width. Linear surface abrasions that occur as swaths of removed tissue between major veins in a parallel-veined leaf (DT366; Fig. 4.11) measure 8.5 mm in length by 1.7 mm in width. Aggregated surface feeding traces, seemingly swollen and of elliptical shape (DT232; Fig. 4.12), measure 6.5 mm in length by 5.9 mm in width, with each individual structure ranging

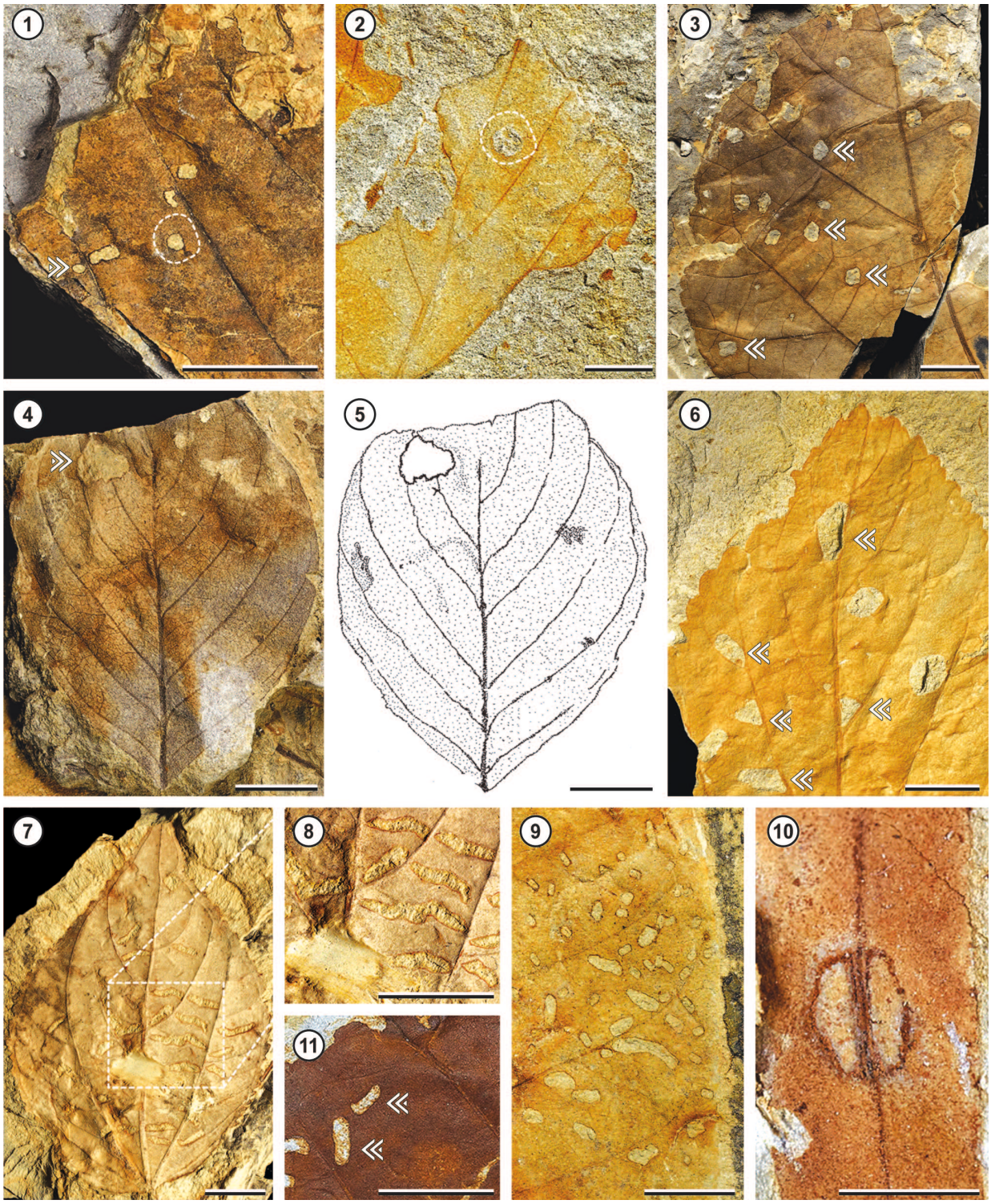

Figure 2. Hole feeding on Paleocene leaves of the Bogotá Formation (Colombia). **1,** Circular holes measuring less than 1 mm in diameter (white arrow; DT1) and between 1 and 5 mm in diameter (dotted line; DT2) on leaf morphotype BF36 (*aff.* Ulmaceae; **STRI** 12107). Scale bar equals 1 cm. **2,** Circular hole greater than 5 mm in diameter (dotted line; DT4) on leaf morphotype BF37 (*aff.* Euphorbiaceae; **STRI** 12278). Scale bar equals 1 cm. **3,** Polylobate holes measuring less than 5 mm in diameter (white arrows; DT3) on leaf morphotype BF4 (Malvaceae; **STRI** 12196). Scale bar equals 1 cm. **4,** Polylobate hole greater than 5 mm in diameter (white arrow; DT5) on leaf morphotype BF7 (Lauraceae; **STRI** 12064). Scale bar equals 1 cm. **5, STRI** 12064-DT5 camera-lucida drawing. Scale bar equals 1 cm. **6,** Holes positioned at intersections between primary and secondary veins (white arrows; DT57) on leaf morphotype BF37 (*aff.* Euphorbiaceae; **STRI** 12295). Scale bar equals 1 cm. **7,** Curvilinear elongate holes with expanding widths (DT7) on leaf morphotype BF23 (*aff.* Salicaceae; **STRI** 12232). Scale bar equals 1 cm. **8, STRI** 12232-DT7 enlarged. Scale bar equals 1 cm. **9,** Cluster of comma shaped holes scattered along leaf margin (dotted line; DT9) on leaf morphotype BF12 (**STRI** 46960). Scale bar equals 1 cm. **10,** Symmetrical perforations occurring on either side of the midvein (DT63) on leaf morphotype BF21 (Fabaceae; **STRI** 12339). Scale bar equals 2 mm. **11,** Elongate parallel-sided holes (DT8) on leaf morphotype BF36 (*aff.* Ulmaceae; **STRI** 12109). Scale bar equals 1 cm.

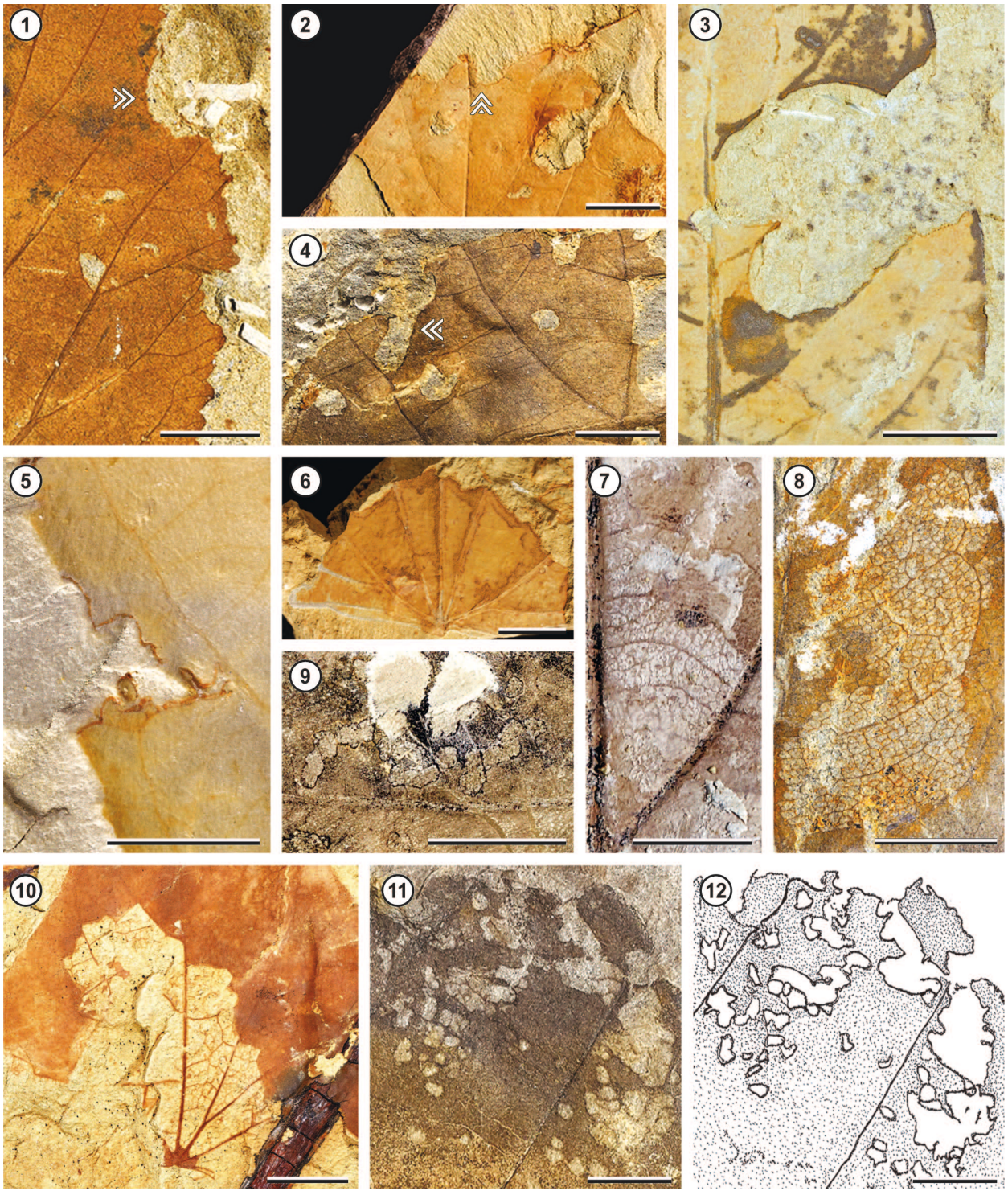

Figure 3. Margin feeding and skeletonization on Paleocene leaves of the Bogotá Formation (Colombia). **1,** Semicircular excision along leaf margin (white arrow; DT12) on leaf morphotype BF37 (*aff.* Euphorbiaceae; **STRI** 12281). Scale bar equals 1 cm. **2,** Excision of leaf apex (white arrow; DT13) on leaf morphotype BF6 (Menispermaceae; **STRI** 12444). Scale bar equals 1 cm. **3,** Excision of leaf margin extending to the midvein (DT14) on leaf morphotype BF16 (**STRI** 12456). Scale bar equals 1 cm. **4,** Excision of leaf margin that changes direction as it expands towards the midvein (white arrow; DT15) on leaf morphotype BF4 (Malvaceae; **STRI** 12196). Scale bar equals 1 cm. **5,** Trenched excision of leaf margin with width expansions and constrictions (DT198) on leaf morphotype BF5 (*aff.* Violaceae/Salicaceae **STRI** 47385). Scale bar equals 5 mm. **6,** Extensive tissue removal leaving remnants of leaf tissue (DT395) on leaf morphotype BF4 (Malvaceae; **STRI** 47370). Scale bar equals 1 cm. **7,** Skeletonized patches with poorly developed reaction rim (DT16) on leaf morphotype BF13 (*aff.* Elaeocarpaceae; **STRI** 47398). Scale bar equals 1 cm. **8,** Skeletonized patches with thick reaction rim (DT17) on leaf morphotype BF38 (Fabaceae; **STRI** 12371). Scale bar equals 5 mm. **9,** Skeletonized curvilinear patches (DT20) on leaf morphotype BF38 (Fabaceae; **STRI** 12399). Scale bar equals 5 mm. **10,** Skeletonized patches occurring around leaf petiole insertion (DT56) on leaf morphotype BF32 (**STRI** 12497). Scale bar equals 1 cm. **11,** Skeletonized leaf margin removing highest order of venation (DT21) on leaf morphotype BF36 (*aff.* Ulmaceae; **STRI** 12107). Scale bar equals 5 mm**. 12, STRI** 12107-DT21 camera-lucida drawing. Scale bar equals 5 mm.

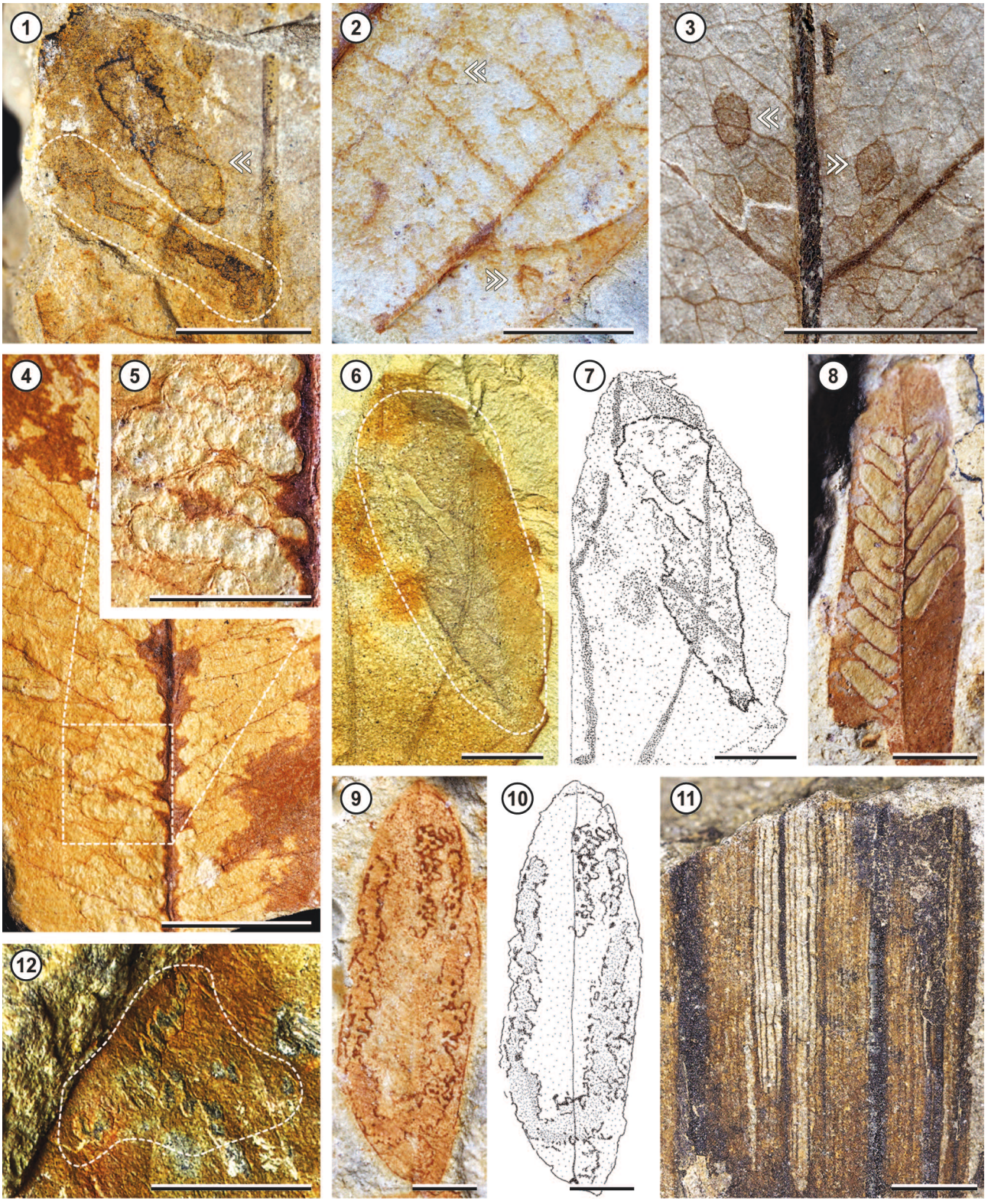

Figure 4. Surface feeding on Paleocene leaves of the Bogotá Formation (Colombia). **1,** Surface abrasion following a linear trajectory on the leaf lamina (dotted line; DT25) and a polylobate abraded patch with a distinct reaction rim (white arrow; DT30) on leaf morphotype BF38 (Fabaceae; **STRI** 12414). Scale bar equals 5 mm. **2,** Polylobate surface abrasion with a poorly developed reaction rim (white arrows; DT29) on leaf morphotype BF13 (*aff.* Elaeocarpaceae; **STRI** 11984). Scale bar equals 5 mm. **3,** Circular to ellipsoidal surface abrasion marks with a distinct reaction rim (white arrows; DT31) on an unidentified leaf morphotype (**STRI** 12658). Scale bar equals 5 mm. **4,** Elongate surface abrasion with thick reaction tissue extending into inner area as wedge-like structures (DT203) on leaf morphotype BF14 (*aff. Phanerophlebia*; **STRI** 13344). Scale bar equals 5 mm. **5, STRI** 13344-DT203 enlarged. Scale bar equals 2 mm. **6,** Very elongate surface abrasion occurring along a leaf margin with poorly developed

0.5–1.1 mm in length and 0.3–0.4 mm in width. Reaction rims associated with surface feeding, when present, are 0.1–0.2 mm thick unless otherwise noted.

Twelve piercing-and-sucking DTs were observed and are illustrated in Figure 5. Circular piercing-and-sucking punctures with a central depression, randomly scattered throughout the leaf (DT46; Fig. 5.1), measure 0.1–0.3 mm in diameter, and similarly shaped piercing-and-sucking punctures with a central dome (DT47; Fig. 5.2) range 0.1–0.4 mm in diameter. Elliptical punctures with a central depression, scattered throughout the lamina (DT48; Fig. 5.3), measure 0.1–0.7 mm in diameter; and circular to elliptical punctures that occur on or along a midvein or a major vein (DT392; Fig. 5.4) measure <0.1 mm in diameter. Aggregated circular scale insect impression marks with one prominent and a subsidiary growth ring (DT77; Fig. 5.5) measure 0.7–1.8 mm in diameter and have a central ring 0.3–0.7 mm in diameter. Elliptical scale-insect impression marks with an eccentrically positioned puncture and distinct reaction rim with a beak (DT128; Fig. 5.6–5.7) measure 3.0 mm in length and 0.9 mm in width and have an inner puncture site that measures 0.4 mm in diameter. Circular or elliptical punctures that occur alongside a midvein or a major vein (DT138; Fig. 5.8–5.9) measure <0.1 mm in diameter. Ellipsoidal to circular scale-insect impression marks that occur as a curvilinear series with reaction rims in contact with each other (DT286; Fig. 5.10) measure 1.3–1.5 mm in length and 0.9–1.4 mm in width. Elliptical to circular punctures that occur as clusters associated with a primary vein and leaf margin (DT281; Fig. 5.11–5.12) measure 0.1–0.3 mm in diameter. Scale-impression marks that occur in groups of various sizes, perhaps reflecting growth increments among instars, and with an overall elliptical (DT132; Fig 5.13) or circular (DT133; Fig. 5.14) shape, measure 0.7–1.7 mm in length and 0.6–1.3 mm in width, for the former, and 0.3–0.5 mm in diameter, for the latter. Solitary, ovoidal scale insect impression marks with a beak in one end and a distinct longitudinal ridge (DT158; Fig. 5.15) measure 6.5 mm long by 3.5 mm in width.

Twenty-four galling DTs are found in the Bogotá flora (Figs. 6–7). Circular, flat galls with thin inner areas, a thick outer rim and an eccentrically positioned dark dot (DT11; Fig. 6.1) measure 3.3–4.6 mm in diameter. Polylobate galls along primary veins (DT33; Fig. 6.2–6.3) measure 1.5–3.0 mm in length by 0.6–1.5 mm in width. Ellipsoidal galls with a large inner carbonized core and a featureless encircling area (DT49; Fig. 6.4–6.5) measure 5.2 mm in length by 5.6 mm in width; these have an inner carbonized core 2.3 mm long by 0.9 mm wide and a reaction rim 0.1–0.2 mm wide. Featureless, circular to ellipsoidal galls on the lamina (DT32; Fig. 6.6–6.7) measure 0.2–2.0 mm in diameter, and circular galls with a central chamber, radiating tissue masses and thick outer wall (DT52; Fig. 6.8), measure 1.3–3.2 mm in length by 1.1–1.9 mm in width. Spheroidal galls positioned on secondary veins, lacking distinguishing features (DT34; Fig. 6.9), measure 0.3–2.0 mm in diameter. A globose gall positioned at a leaf petiole (DT55; Fig 6.10) measures 5.6 mm in length by 3.2 mm in width. Triangular galls with an eccentric inner chamber and a poorly developed outer wall (DT62; Fig. 6.11) range 0.6–3.1 mm in diameter, and shallow hemispheroidal galls with a smooth outer surface that avoid major veins (DT80; Fig. 6.12) measure 0.8–1.9 mm in diameter. Circular flat galls with a carbonized core and a very thick outer zone (DT83; Fig. 6.13) measure 1.6–4.3 mm in diameter. Lenticular galls along major veins (DT85; Fig. 6.14) are 3.4–3.8 mm long by 0.9–2.9 mm wide. Discoidal galls adjacent to primary veins with a thick outer wall (DT120; Fig. 6.15) measure 1.6–2.8 mm in diameter, with a reaction rim 0.2–0.3 mm wide. Compound galls consisting of minute, minuscule chambers clustered in a single structure (DT107; Fig. 6.16–6.17) are 12.1 mm long by 8.4 mm wide; each individual chamber is 0.2–0.3 mm in diameter. Bulbous ellipsoidal galls with a thick wall and radiating structures with a pustulose surface (DT127; Fig. 7.1) measure 4.5 mm in length by 3.5 mm in width, and its radiating

Figure 4. Continuation.
reaction rim (dotted line; DT155) on leaf morphotype BF37 (*aff.* Euphorbiaceae; **STRI** 46989). Scale bar equals 5 mm. **7, STRI** 46989-DT155 camera-lucida drawing. Scale bar equals 5 mm. **8,** Surface abrasion consisting of numerous slots adjacent and parallel to major veins, with extensive rim tissue and length width ratios greater than 2.5 (DT317) on leaf morphotype BF21 (Fabaceae; **STRI** 47674). Scale bar equals 2 mm. **9,** Irregular, linear swaths of surface abrasion running along the leaf margin with wedge-like extensions into inner area (DT365) on leaf morphotype BF21 (Fabaceae; **STRI** 12328). Scale bar equals 1 mm. **10, STRI** 12328-DT365 camera-lucida drawing. Scale bar equals 1 mm. **11,** Surface abrasion occurring as linear swaths between primary and secondary veins in a parallel-veined leaf (DT366) on leaf morphotype BF27 (Arecaceae; **STRI** 12486). Scale bar equals 2 mm. **12,** Surface abrasion consisting of aggregated swollen ellipsoidal structures with smooth surfaces (dotted line; DT232) on leaf morphotype BF12 (**STRI** 46954). Scale bar equals 5 mm.

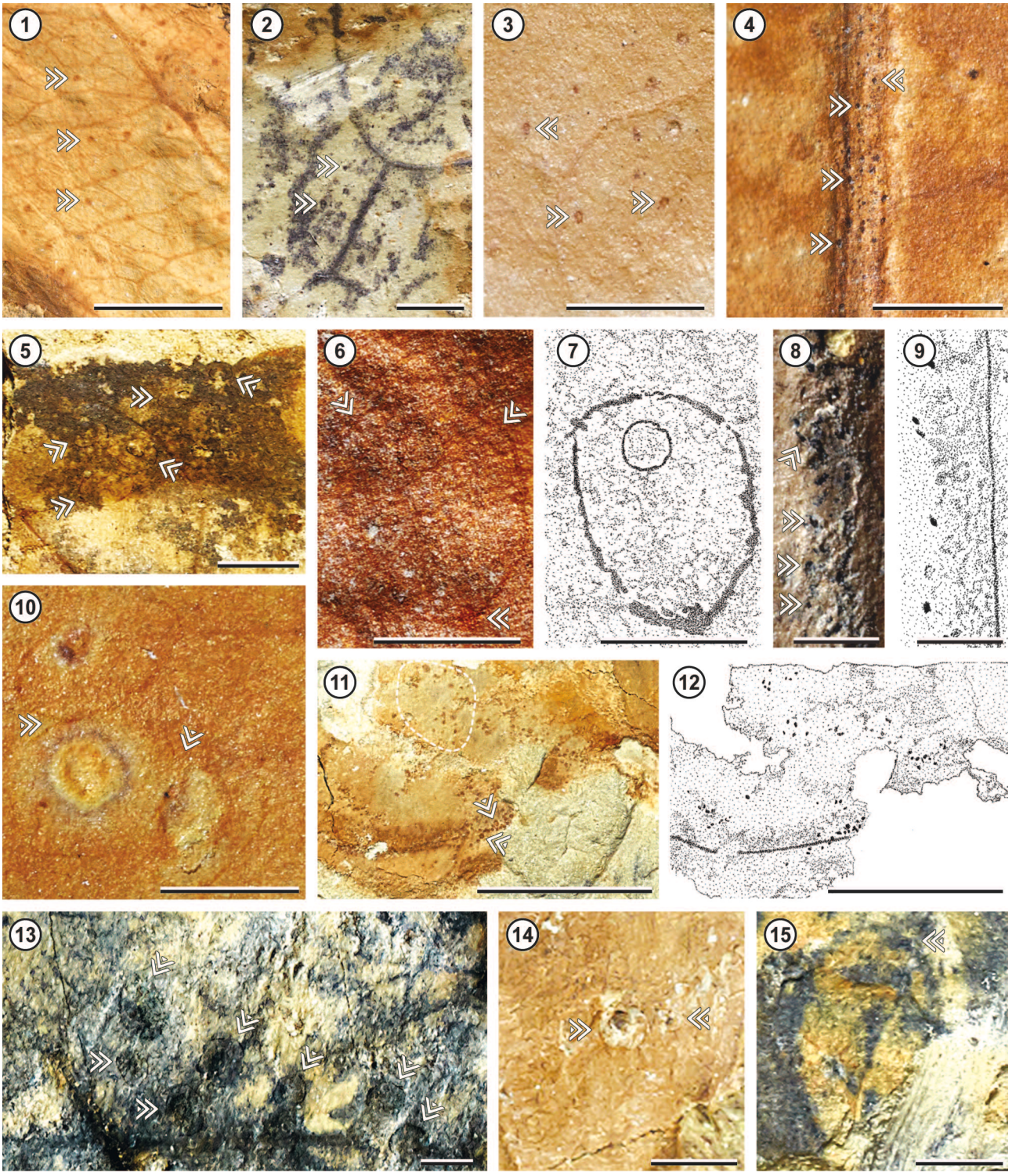

Figure 5. Piercing-and-sucking traces on Paleocene leaves of the Bogotá Formation (Colombia). **1,** Numerous circular piercing-and-sucking punctures characterized by a central depression, randomly positioned along the lamina (white arrows; DT46) on leaf morphotype BF15 (**STRI** 12455). Scale bar equals 5 mm. **2,** Two circular piercing-and-sucking punctures with a central dome (white arrows; DT47), located on the lamina of leaf morphotype BF4 (Malvaceae; **STRI** 12199). Scale bar equals 5 mm. **3,** Elliptical piercing-and-sucking punctures characterized by a central depression (white arrows; DT48), positioned on the lamina of leaf morphotype BF4 (Malvaceae; **STRI** 12220). Scale bar equals 2 mm. **4,** A row of numerous circular to elliptical piercing-and-sucking punctures occurring on and along the midvein (white arrows, DT392) on leaf morphotype BF42 (**STRI** 47390). Scale bar equals 2 mm. **5,** Circular scale insect impression marks occurring as clusters of a few individuals. Each scale consists of an outer (white arrows) and inner ring (DT77) on leaf morphotype BF4 (Malvaceae; **STRI** 12216). Scale bar equals 5 mm. **6,** Elliptical scale insect impression mark with discernable border (upper arrows), characterized by an apical beak (lower arrow) and an eccentrically positioned puncture (DT128) on leaf morphotype BF47 (**STRI** 13317). Scale bar equals 1 mm. **7, STRI** 13317-DT128 camera-lucida drawing. Scale bar equals 1 mm.

structures are 0.4–2 mm long and 0.3 mm wide. Robust galls, positioned on a primary vein, with a thickened base and a smooth surface (DT146; Fig. 7.2), are 3.7–9.2 mm long by 1.6–8.9 mm wide. Cylindrical galls with a hemispheroidal upper region (DT149; Fig. 7.3–7.4) are 2.5 mm long by 1.6 mm wide. Circular galls with a thick outer rim and radiating pustulose structures (DT163; Fig. 7.5) measure 4.1 mm in length by 3.5 mm in width, and each pustule is 0.2–0.3 mm in diameter. Polylobate galls with carbonized impressed material (DT303; Fig. 7.6) are 0.8–2.1 mm long by 0.6–1.8 mm wide; and bulbous galls that deform leaf shape and venation, have a thick sinuate margin and a central raised area (DT397; Fig. 7.7) measure 4.3 mm in diameter. Torus-like galls with radiating ridges that emerge from a central depression (DT194; Fig. 7.8) measure 2.1 mm in length by 1.5 mm in width; each ridge is 0.4–0.6 mm long and 0.1 mm wide and the inner depression is 0.4 mm in diameter. Aggregated ellipsoidal galls, 4.5–5.3 mm long by 2.7–3.0 mm wide, with a pustulose surface are positioned adjacent to major veins (DT 289; Fig. 7.9). A series of 7.3–8.5 mm long and 5.6–7 mm wide lenticular galls aligned along a primary vein, have a roughened central area and a thick wall (DT241; Fig. 7.10–7.11). Aggregated, 0.2–1.6 mm wide hemispheroidal galls with a broad featureless zone of altered host tissue and accompanied by an eccentrically positioned central chamber (DT265; Fig. 7.12), measure 1.5–4.4 mm in length by 0.9–2.2 mm in width. A compound polylobate gall with development of corky tissue and with several minute chambers (DT254; Fig. 7.13–7.14) measures 11.1 mm in length by 4.6 mm in width, and each chamber is <0.1 mm in diameter.

Six oviposition DTs were observed in the Bogotá flora and are illustrated in Figure 8. Elliptical oviposition scars aligned widthwise to each other form two distinct curvilinear rows (DT54; Fig. 8.1), one 5.4 mm long (upper arrow) and the other 3.8 mm in length (lower arrow). Each oviposition scar has a length-to-width ratio of 2.1 and a distinct reaction rim <0.1 mm wide (Fig. 8.2–8.3). Lenticular oviposition scars occur along the midvein (DT72; Fig. 8.4), 3.4 mm long by 1.5 mm wide, with outer and inner reaction rims, both <0.1 mm wide. Possible coleophorid moth cases–cylindrically-shaped structures with one truncated end and the other with a rounded border–oriented along and parallel to the leaf margin (DT364; Fig. 8.5) measure 1.5 mm in width and 2.3–4.2 mm in length. A row of 11 ellipsoidal oviposition lesions occurring lengthwise aligned along the midvein (DT76, Fig. 8.6), measure 8.4 mm in total length, with each scar separated by 0.2–0.4 mm. Each lesion has a length-to-width ratio of 2.1 and reaction tissue <0.1 mm wide. A circular to slightly elliptical oviposition scar with a distinct reaction rim and a central depression, positioned along the midvein (DT228; Fig. 8.7–8.8), has a diameter of 1 mm and a raised outer rim 0.1 mm in height. Elliptical oviposition scars occurring lengthwise along the midvein, with four internal structures bounded by a raised border (DT396; Fig. 8.9) measure 3.2–3.4 mm long by 1.5–2.2 mm wide. The raised border is 0.1 mm in height and is maintained by the internal separation of the structure, which in turn are triangular to elliptical in shape, with length-to-width ratios of 1.1–2.1

Four pathogen DTs are observed in the Bogotá flora and are illustrated in Figure 8. Polylobate blotches with dark diffuse reaction rims fronts or rims (DT58; Fig. 8.10) measure 1.3–41.5 mm in length and 1.1–21.1 mm in width. Densely packed clusters of circular to ovoidal necrotic blotches with rounded and diffuse reaction fronts (DT69; Fig. 8.11–8.12) consist of pathogenic structures that measure 0.1–4 mm, with aggregates up to 3 cm. Concentric pustules (pycnidia?) that are circular to ellipsoidal in shape are positioned adjacent to secondary veins (DT66, Fig. 8.13–8.14), and

Figure 5. Continuation.
8, A row of circular to elliptical piercing-and-sucking punctures occurring alongside the midvein (white arrows; DT138) on leaf morphotype BF13 (*aff.* Elaeocarpaceae; **STRI** 47398). Scale bar equals 0.5 mm. **9, STRI** 47398-DT138 camera-lucida drawing. Scale bar equals 0.5 mm. **10,** A curvilinear series of three ellipsoidal scale insect impression marks. Each scale is characterized by a distinct reaction rim that appears in contact with one another (white arrows; DT286) on leaf morphotype BF4 (Malvaceae; **STRI** 12220). Scale bar equals 1 mm. **11,** Elliptical to circular piercing-and-sucking punctures associated with a primary vein and leaf margin. Punctures in proximity of the vein (white arrows) have greater diameters than those located in the lamina (dotted line; DT281), on leaf morphotype BF4 (Malvaceae; **STRI** 46990). Scale bar equals 5 mm. **12, STRI** 46990-DT281 camera-lucida drawing. Scale bar equals 5 mm. **13**, Groups of elliptical scale-impression marks with different sizes (white arrows; DT132), perhaps reflecting instars, on leaf morphotype BF5 (*aff.* Violaceae/Salicaceae; **STRI** 46983). Scale bar equals 2 mm. **14**, Circular scale-impression marks with different sizes and distinct reaction rims (white arrows; DT133) on leaf morphotype BF62 (**STRI** 46953). Scale bar equals 1 mm. **15**, Ovoidal scale insect impression mark with a beak in one end (white arrow) and a distinct longitudinal ridge (DT158) on leaf morphotype BF62 (**STRI** 46966). Scale bar equals 2 mm.

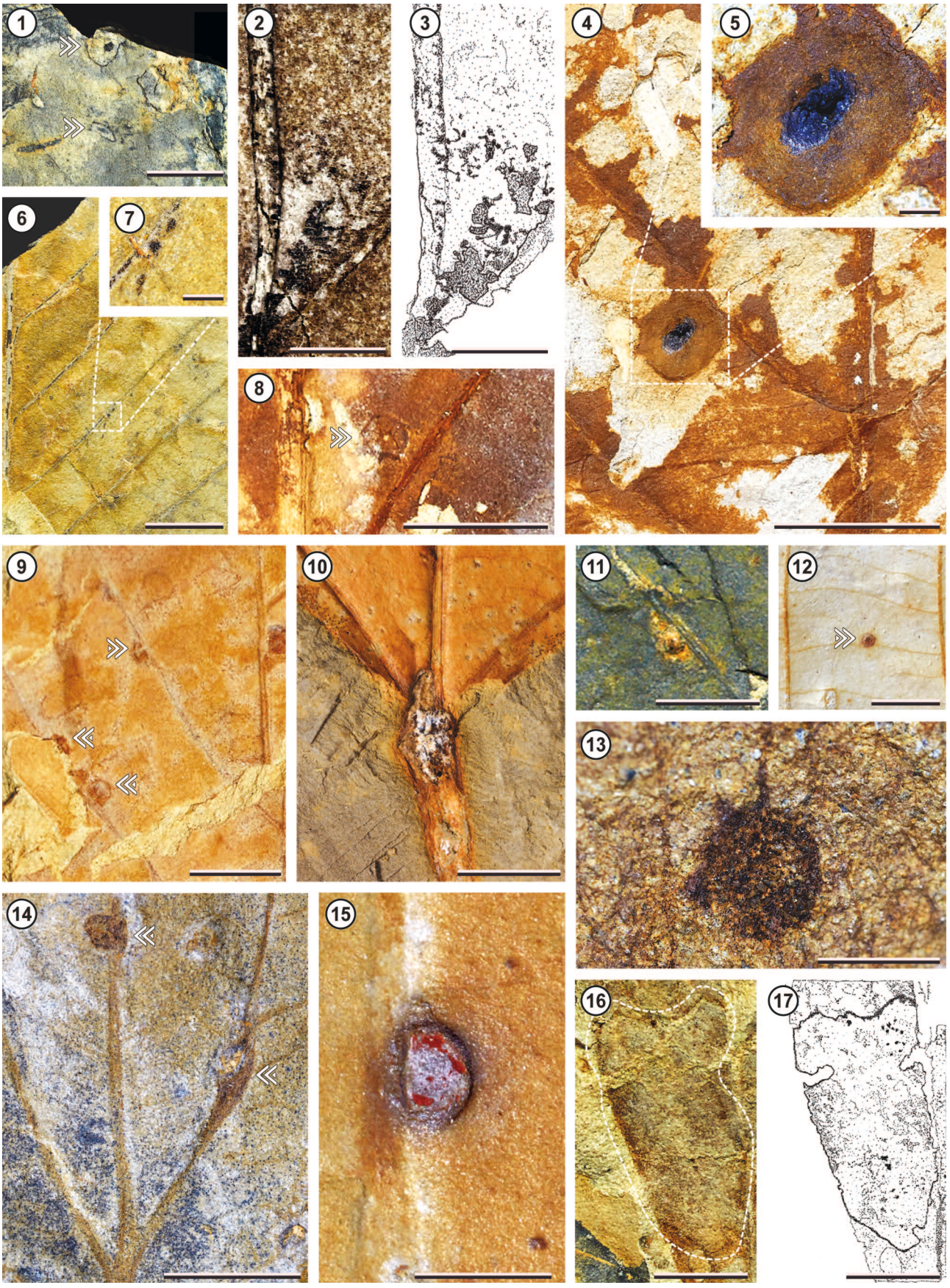
1
2
3
4
5
6
7
8
9
10
11
12
13
14
15
16
17

measure 2.2–5.8 mm in diameter. Each of these pustules is circular, 0.1–0.2 mm in diameter; or elliptical, and measure 0.1–0.5 mm in length and 0.1–0.2 mm wide. Other pathogen damage consists of linear necrotic blotches that follow primary veins and damaged margins (DT390; Fig. 8.15), representing secondary infection, and have dark reaction fronts 0.1–0.2 mm thick and width constrictions ranging from 0.7–1.7 mm.

Mine descriptions by leaf morphotype

There are 13 mine DTs that have been recovered from the Bogotá flora, described in detail below, one of which (DT367) is new and not previously recorded from any known flora.

Morphotype BF4. The leaf morphotype BF4 bears three leaf-mine DTs. The mine assigned to DT105 (Fig 9.1) is a serpentine mine 40.9 mm long, characterized by several 90° turns, parallel lateral sides and a trajectory limited by primary and tertiary veins. The mine has no discernable oviposition site and was initiated next to a primary vein, which follows for 5.6 mm. The mine reorients by forming a 90° angle and continuing to follow a tertiary vein for 12.5 mm until reaching the next primary vein. The mine bends at a 90° angle and follows the primary vein towards the leaf base for 4 mm before it is redirected and follows yet another tertiary vein for 11.9 mm, and then contacts a third primary vein. The mine undergoes one last 90° bend and follows the primary vein towards the leaf apex for 4.4 mm to reach a circular terminal chamber 1.9 mm in diameter. The mine is 0.3 mm wide throughout its course and lacks instar-related width increases.

Two leaf mines assigned to DT109 (Fig. 9.2) are characterized by being thin and threadlike, with their trajectory bounded by tertiary veins. They contain minute spheroidal to broadly ellipsoidal frass pellets <0.1 mm in diameter. The first mine (upper arrow) is 9.6 mm long and courses halfway through a tertiary vein, with a width of 0.1 mm. This mine follows the tertiary vein for 4.5 mm until reaching a secondary vein. At this point, the mine width enlarges to 0.2 mm and reorients following a curvilinear path towards the mine's oviposition site. The mine terminates at a 0.6 mm long by 0.3 mm wide, elliptical terminal chamber. The second DT109 mine (lower arrow) is 13.9 mm long and originates at the junction between a secondary and tertiary vein. The mine follows and crosses this tertiary vein until reaching a secondary vein and increases its width to 0.1mm; then the mine makes a U-turn, crosses over the first mine's path, and its path becomes sinusoidal. No terminal chamber is associated with this mine.

Lastly, a newly reported leaf mine in this flora is assigned to DT367 (Fig. 9.3). It consists of a robust, gently serpentine mine 47.4 mm in total length, characterized by its prominent reaction rim, a trajectory limited by primary and secondary venation and possessing seemingly fluidized frass. The mine's initial phase consists of a curvilinear path 11.4 mm in length, with diffuse reaction tissue and a constant width of 0.5 mm. Then, the mine quickly expands to a width up to 1.5 mm with massive reaction tissue 0.6 mm in height; it follows a curvilinear path for 5.5 mm until reaching a primary vein, where it bifurcates. One branch follows a 4.2 mm path and ends with a rounded border. The other branch continues the mine, following the primary vein for

Figure 6. Galling on Paleocene leaves of the Bogotá Formation (Colombia). **1,** Two flat galls with a thin inner area, characterized by an eccentrically positioned dark dot and delimited by a ring of hardened tissue (white arrows; DT11) on leaf morphotype BF33 (Euphorbiaceae; **STRI** 46964). Scale bar equals 1 cm. **2,** Polylobate gall positioned along primary and secondary vein junction (DT33) on leaf morphotype BF36 (*aff.* Ulmaceae; **STRI** 12106). Scale bar equals 1 mm. **3, STRI** 12106-DT33 camera-lucida drawing. Scale bar equals 1 mm. **4,** Ellipsoidal gall with a large central carbonized core, encircled by a featureless area (DT49) on leaf morphotype BF36 (*aff.* Ulmaceae; **STRI** 12109). Scale bar equals 1 cm. **5, STRI** 12109-DT49 enlarged. Scale bar equals 1 mm. **6,** Circular to ellipsoidal foliar galls, without distinctive features (DT32) on leaf morphotype BF5 (*aff.* Violaceae/Salicaceae **STRI** 46987). Scale bar equals 5 mm. **7, STRI** 46987-DT32 enlarged. Scale bar equals 1 mm. **8,** Circular to squarose gall with a central chamber surrounded by radiating masses and an outer wall (white arrow; DT52) on leaf morphotype BF13 (*aff.* Elaeocarpaceae; **STRI** 12004). Scale bar equals 1 cm. **9,** Spheroidal to ellipsoidal galls occurring on secondary veins, lacking distinguishing features (white arrows; DT34) on leaf morphotype BF13 (*aff.* Elaeocarpaceae; **STRI** 11977). Scale bar equals 5 mm. **10,** Globose gall occurring on leaf petiole (DT55) on leaf morphotype BF5 (*aff.* Violaceae/Salicaceae; **STRI** 12443). Scale bar equals 5 mm. **11,** Triangular gall with eccentric inner chamber and poorly developed outer wall (DT62) on leaf morphotype BF37 (*aff.* Euphorbiaceae; **STRI** 47124). Scale bar equals 5 mm. **12,** Shallow hemispheroidal gall avoiding major veins, with smooth outer surface (white arrow, DT80) on leaf morphotype BF5 (*aff.* Violaceae/Salicaceae; **STRI** 12084). Scale bar equals 5 mm. **13,** Circular flat gall, with a carbonized core and thick outer zone (DT83) on leaf morphotype BF38 (Fabaceae; **STRI** 12396). Scale bar equals 2 mm. **14,** Lenticular gall positioned lengthwise in a major vein (white arrows; DT85) on leaf morphotype BF37 (*aff.* Euphorbiaceae; **STRI** 12263). Scale bar equals 5 mm. **15,** Discoid gall adjacent to a primary vein, with thick outer wall (DT120) on leaf morphotype BF4 (Malvaceae; **STRI** 12220). Scale bar equals 1 mm. **16,** Compound gall consisting of many minuscule chambers clustered in a single structure (dotted line; DT107) on leaf morphotype BF39 (**STRI** 46969). Scale bar equals 5 mm. **17, STRI** 46969-DT107 camera-lucida drawing. Scale bar equals 5 mm.

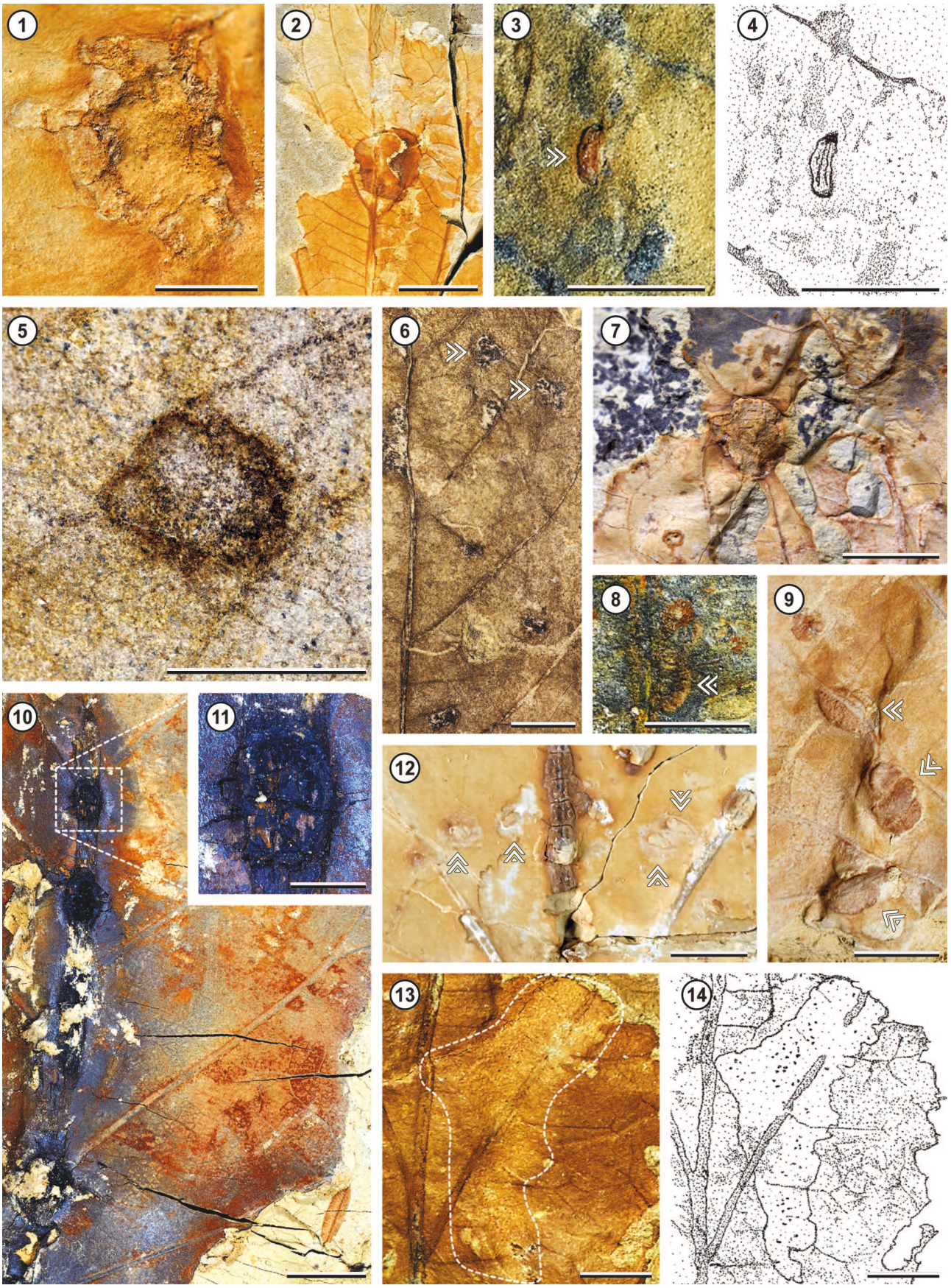
1
2
3
4
5
6
7
8
9
10
11
12
13
14

9.8 mm up to the junction with a secondary vein. There, the mine reorients towards the interveinal tissue with a 45° angle turn and follows a sinusoidal path for 14.8 mm, with consistent width constrictions and expansions from 0.4–1.5 mm in width. At that point the mine shrinks in width and assumes the 0.5 mm width of the initial phase of the mine. The mine then follows a linear path for 1.7 mm before its termination. There is no evidence of a terminal chamber or exit slit; it appears that this is an aborted beetle mine.

Morphotype BF7. The leaf morphotype BF7 has one mine occurrence assigned to DT90 (Fig. 9.4–9.5), characterized by a curvilinear trajectory, gradual width increases and generalized lack of frass. The mine originates (white lower arrow) with a 0.2 mm width, follows a linear path for 1 mm, and turns towards a secondary vein for 2.7 mm, where the mine expands to its final width of 0.7 mm. The mine continues along and adjacent to the secondary vein for 5.5 mm and terminates at a rounded border, but without a distinct terminal chamber. Although no frass trail is discernible, some ellipsoidal coprolites <0.1 mm (white upper arrows) are dispersed along the last portion of the mine.

Morphotype BF11. The only leaf mine associated to BF11 is DT99 (Fig. 9.6), a linear mine 6.2 mm long, having a gradual width increase and mostly confined to the leaf margin. Even though the mine is incomplete, it has an initial width of 0.2 mm and is observed next to the midvein (white arrow) and follows an arcuate path of 1.7 mm towards the leaf margin. The mine increases in width as it follows the leaf margin, reaching a maximum width of 0.5 mm at the leaf base. No clear frass trail or terminal chamber are evident in this mine.

Morphotype BF13. Leaf morphotype BF13 has two mine occurrences. The first leaf mine, DT139 (Fig. 9.7–9.8), is a 14 mm long, tortuous, wide mine, characterized by a sinuate margin of variable width and an undulatory frass trail that occupies the entire width of the mine. The mine has an initial width of 0.7 mm and follows a linear path of 2.9 mm. At this point, the mine has increased to 1.8 mm in width, makes a 90° turn, and crosses over a secondary vein. A serpentine deployed frass trail is clearly visible (between white arrows) that occupies the entire width of the mine and has a regular crest-to-crest distance of 1.4 mm. The terminal chamber is elliptical, 3.7 mm long by 3.1 mm wide.

The second leaf mine associated with BF13 is a linear mine, 22.6 mm long and characterized by a constant width increase and absence of frass, assigned to DT152 (Fig. 9.9). The mine is located in interveinal tissue close to the leaf margin and starts with a width of 0.7 mm (leftmost arrow). After 18.7 mm of coursing, the mine reaches a blotch-like phase (rightmost arrow). This blotch is squarose in overall shape, 3.9 mm long by 2.3 mm wide, and has a discernable reaction border 0.1 mm wide.

Morphotype BF23. Leaf morphotype BF23 has one mine occurrence, assigned to DT44 (Fig. 9.10). The mine is short and serpentine, 10 mm long, characterized by an expanding and contracting width and a trajectory that is limited by a primary vein. The mine has an initial width of 0.3 mm and originates adjacent to a primary vein, near the leaf base. The mine width undergoes two cycles of expansion and contraction along 7 mm of the mine's trajectory: the mine increases in width to 0.9 mm, then decreases to 0.6 mm, and subsequently increases to 1.5 mm in width before reaching 1 mm in width at the neck of the terminal chamber. The mine terminates in an empty, rounded terminal chamber that is 2.3 mm wide by 3 mm long.

Figure 7. Galling (continued) on Paleocene leaves of the Bogotá Formation (Colombia). **1,** Bulbous ellipsoidal gall with a thick wall and coarsely dimpled radiating structures (DT127) on leaf morphotype BF34 (**STRI** 12498). Scale bar equals 2 mm. **2,** Robust gall with a thickened base and smooth surface, situated on a primary vein (DT146) on leaf morphotype BF37 (*aff.* Euphorbiaceae; **STRI** 12287). Scale bar equals 1 cm. **3,** Cylindrical gall with a hemispheroidal upper region (white arrow, DT149) on leaf morphotype BF60 (**STRI** 46958). Scale bar equals 5 mm. **4, STRI** 46958-DT149 camera-lucida drawing. Scale bar equals 5 mm. **5,** Circular gall with a very thick outermost rim and radially arranged pustulose structures (DT163) on leaf morphotype BF13 (*aff.* Elaeocarpaceae; **STRI** 12050). Scale bar equals 5 mm. **6,** Polylobate galls with striated carbonized material (white arrows; DT303) on leaf morphotype BF36 (*aff.* Ulmaceae; **STRI** 12106). Scale bar equals 5 mm. **7,** Bulbous gall with a thick sinuate margin, deforming leaf shape and venation (DT397) on leaf morphotype BF4 (Malvaceae; STRI 12224). Scale bar equals 5 mm. **8,** Torus-like gall with radiating ridges emerging from central depression (white arrow; DT194) on leaf morphotype BF12 (**STRI** 46943). Scale bar equals 5 mm. **9,** Aggregated ellipsoidal galls (or double gall; lowermost arrow) with pustulose surface, adjacent to major veins (white arrows; DT289) on leaf morphotype BF13 (*aff.* Elaeocarpaceae; **STRI** 11977). Scale bar equals 5 mm. **10,** Series of lenticular galls positioned lengthwise in a primary vein, with roughened central area and thick wall (DT241), on leaf morphotype BF13 (*aff.* Elaeocarpaceae; **STRI** 12002). Scale bar equals 1 cm. **11, STRI** 12002-DT241 enlarged. Scale bar equals 1 mm. **12,** Aggregated hemispheroidal galls with a broad zone of altered host tissue (white arrows) and an eccentrically positioned central chamber (DT265) on leaf morphotype BF4 (Malvaceae; **STRI** 12194). Scale bar equals 5 mm. **13,** Compound robust gall with development of corky tissue and several minuscule chambers (dotted line; DT254) on leaf morphotype BFM2 (**STRI** 46953). Scale bar equals 2 mm. **14, STRI** 46953-DT254 camera-lucida drawing. Scale bar equals 2mm.

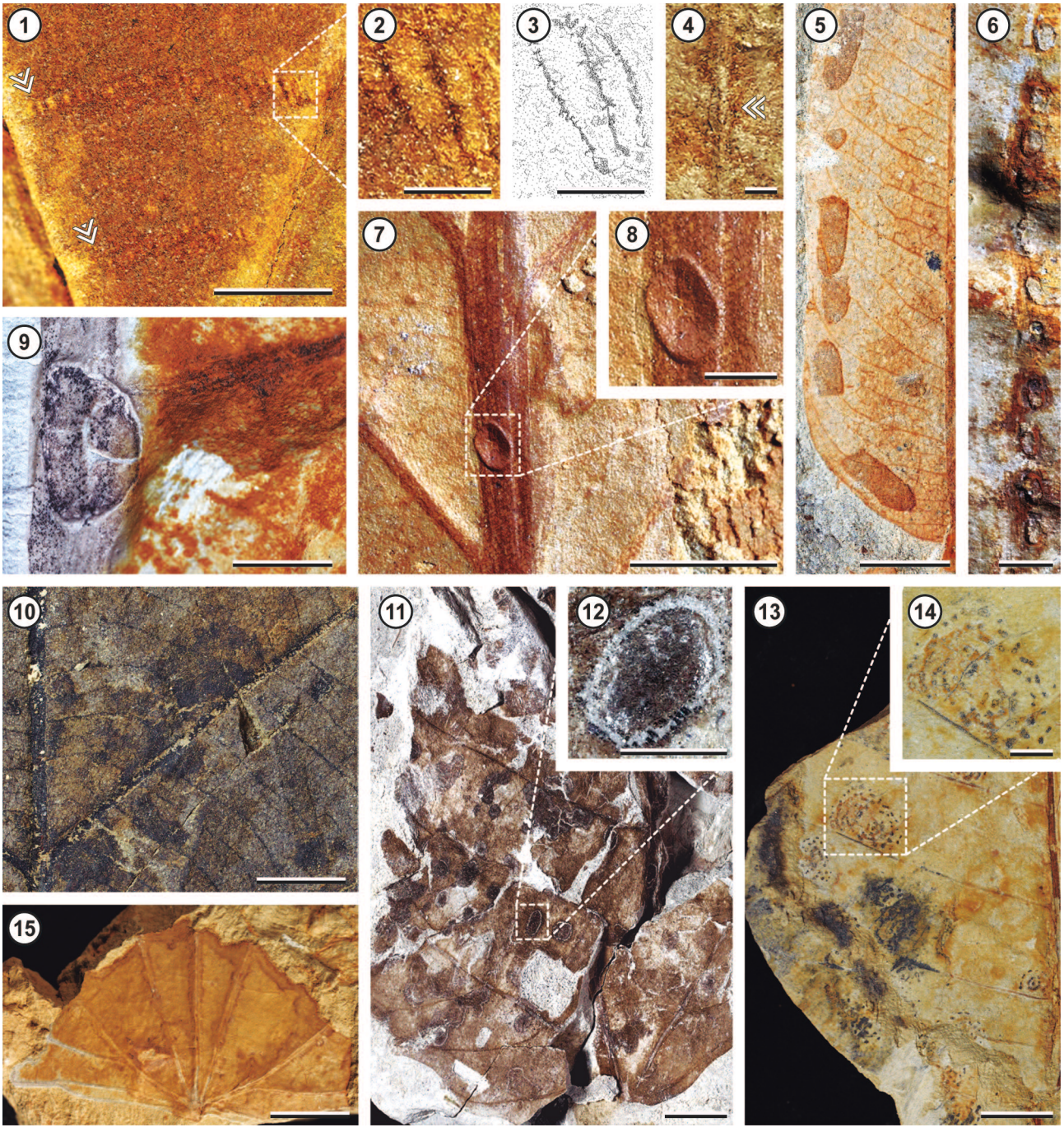

Figure 8. Oviposition and pathogen damage on Paleocene leaves of the Bogotá Formation (Colombia). **1,** Elliptical oviposition scars aligned widthwise to each other, forming two distinct rows (white arrows; DT54) on leaf morphotype BF13 (*aff.* Elaeocarpaceae; **STRI** 12014). Scale bar equals 2 mm. **2, STRI** 12014-DT54 enlarged. Scale bar equals 0.2 mm. **3, STRI** 12014-DT54 camera-lucida drawing. Scale bar equals 2 mm. **4,** Lenticular oviposition scar occurring along the midvein, with a distinct reaction tissue (DT72) on leaf morphotype BF39 (**STRI** 46969). Scale bar equals 2 mm. **5,** Cylindrical-shaped coleophorid cases (?) oriented close and parallel to leaf margin (DT364) on leaf morphotype BF38 (Fabaceae; **STRI** 12349). Scale bar equals 5 mm. **6,** A row of ellipsoidal oviposition lesions with prominent reaction tissue, occurring alongside and lengthwise aligned to the midvein (DT76) on an unidentified leaf morphotype (**STRI** 46697). Scale bar equals 1 mm. **7,** Circular to slightly elliptical oviposition scar with thick reaction rim and a central depression, occurring along the midvein (DT228) on leaf morphotype BF15 (**STRI** 12455). Scale bar equals 5 mm. **8, STRI** 12455-DT228 enlarged. Scale bar equals 1 mm. **9,** Elliptical oviposition scar occurring lengthwise along the midvein, with a prominent raised border and 4 internal structures (DT396) on leaf morphotype BF2 (*aff.* Salicaceae**; STRI** 47371). Scale bar equals 2 mm. **10,** Pathogenic damage consisting of a polylobate blotch with a dark, diffuse reaction front (DT58) on leaf morphotype BF13 (*aff.* Elaeocarpaceae; **STRI** 12059). Scale bar equals 1 cm. **11,** Circular to ovoidal blotches with a rounded and diffuse reaction front, occurring in densely packed clusters (DT69) on leaf morphotype BF36 (*aff.* Ulmaceae; **STRI** 12110). Scale bar equals 1 cm. **12, STRI** 12110-DT69 enlarged. Scale bar equals 1 mm. **13,** Concentric pustules (pycnidia?), circular to ellipsoidal in shape, occurring on the leaf lamina and adjacent to secondary veins (DT66) on leaf morphotype BF51 (**STRI** 46944). Scale bar equals 5 mm. **14, STRI** 46944-DT66 enlarged. Scale bar equals 1 mm. **15,** Pathogenic damage consisting of linear blotches that follow primary veins and damaged margin with a clear reaction front (DT390) on leaf morphotype BF4 (Malvaceae; **STRI** 47370). Scale bar equals 1 cm.

Morphotype BF38. The leaf morphotype BF38 is associated with one mine assigned to DT177 (Fig. 9.11–9.12). This is a meandering mine 15.7 mm long, characterized by a tight 180° turn midway through its course and having consistently parallel borders. No oviposition site is evident for this mine, which has a constant width of 0.4 mm and begins in an interveinal area. The mine follows a sinusoidal path for 7.8 mm; initially lacks frass but gradually becomes filled with spheroidal to ellipsoidal frass pellets <0.1 mm in diameter that cover the entire width of the mine. After the tight 180° turn, the mine follows a linear path of 5 mm as it approaches the neck of the terminal chamber. The chamber is elliptical in shape, 1.2 mm long and 0.7 mm wide.

Morphotype BF41. A leaf mine assigned to DT37 (Fig. 10.1) is found on leaf morphotype BF41. DT37 is an elongate, polylobate blotch mine located between two secondary veins, characterized by a 26.7 mm long, tightly packed, sinusoidal frass trail. The mine originates as a thread-like structure <0.1 mm wide that forms a hairpin loop and reorients towards the primary vein. At this point, the mine contains a 0.1 mm wide frass trail and follows the primary and superjacent secondary vein, to then reorient again towards the primary vein in an arcuate trajectory. Then, the mine follows a sinusoidal path from the midvein towards the subjacent secondary vein, leaf margin and superjacent secondary vein, forming an 8.2 mm long by 6 mm wide polylobate central chamber that is bounded by major veins. During the course of the mine, the frass trail increased from a width of 0.1 mm to 0.3 mm and shows a clear sinusoidal trajectory. The mine continues to follow the superjacent secondary vein towards the midvein until it reaches an earlier stage of the leaf mine, and ends in a coiled trajectory within the central chamber where the frass trail reaches a maximum width of 0.4 mm.

Morphotype BF42. The leaf morphotype BF42 has two mine occurrences. The first leaf mine, assigned to DT43 (Fig. 10.2), is a short 23 mm long serpentine mine, characterized by parallel lateral margins and a frass trail of solid coprolites that occupies the entire mine. The mine has an initial width of 0.7 mm and originates between two secondary veins close to the leaf apex. The mine increases in width as it follows a serpentine path towards the leaf margin and turns towards the leaf apex for 5 mm. At this point, the mine has increased to a width of 1 mm and turns towards the midvein, following a sinusoidal path of 5.8 mm. Individual frass pellets are discernable and have an ellipsoidal shape and length-to-width ratios of 1.2–1.5. After reaching the midvein, the mine reorients 180° towards the leaf margin along a 5.8 mm stretch. The frass becomes liquified (lower white arrow) as the mine shifts 75° towards the leaf apex and terminates at a broadly circular chamber (upper white arrow) of 2.7 mm in diameter.

The second leaf mine found on BF42 is an asteronome mine 12.6 mm long, characterized by frequent bifurcations, course reversals and mine reoccupation, assigned to DT207 (Fig. 10.3–10.4). The mine lacks a clear oviposition site, and reconstruction of the mine trajectory is difficult, given the evident path reversals. The mine is located between two secondary veins, has a constant width of 0.1 mm, and has a consistent pattern of arcuate trajectories of varying lengths, all of which are directed towards the leaf apex.

Unidentified leaf morphotype. Leaf mine DT234 (Fig. 10.5–10.6) is associated with an unidentified leaf morphotype. DT234 is characterized by a trajectory that is limited by venation, has dark borders and terminates in circular chamber. Lacking a distinct oviposition site, the mine originates on interveinal tissue and has an initial width of 0.1 mm. The mine follows a curvilinear path towards the secondary vein for 1.2 mm and follows a trajectory for 1.1 mm until reaching a tertiary vein. The path reorients to follow the tertiary vein and expands to 0.2 mm in width, and terminates at a circular terminal chamber, 0.7 mm in diameter, with prominent reaction tissue that is 0.2 mm thick. No conspicuous frass trail is observed along this mine, and this absence likely is a taphonomic artifact.

Frequency and richness of damage types

A high percentage of leaves exhibit herbivory-related damage. Based on the means of 5000 iterations of 400 randomly sampled leaves, 69.5 (± 1.7%) of the leaves have some instance of insect-feeding damage; 38.2 (± 1.8%) have specialized DTs (HS = 2–3), and 9.6 (± 1.1%) show highly specialized DTs (HS = 3). Noticeably, 17.1 (± 1.4%) of leaves have galls and 1.8 (± 0.5%) have mines. More than half of the leaves (50.6%) have at least two or more DTs and up to 11 DTs were observed on a single leaf. On average, 61.0 (± 3.3) distinct DTs are observed across 400 randomly sampled leaves; 35.0 (± 2.6) of these are specialized DTs (HS = 2–3)

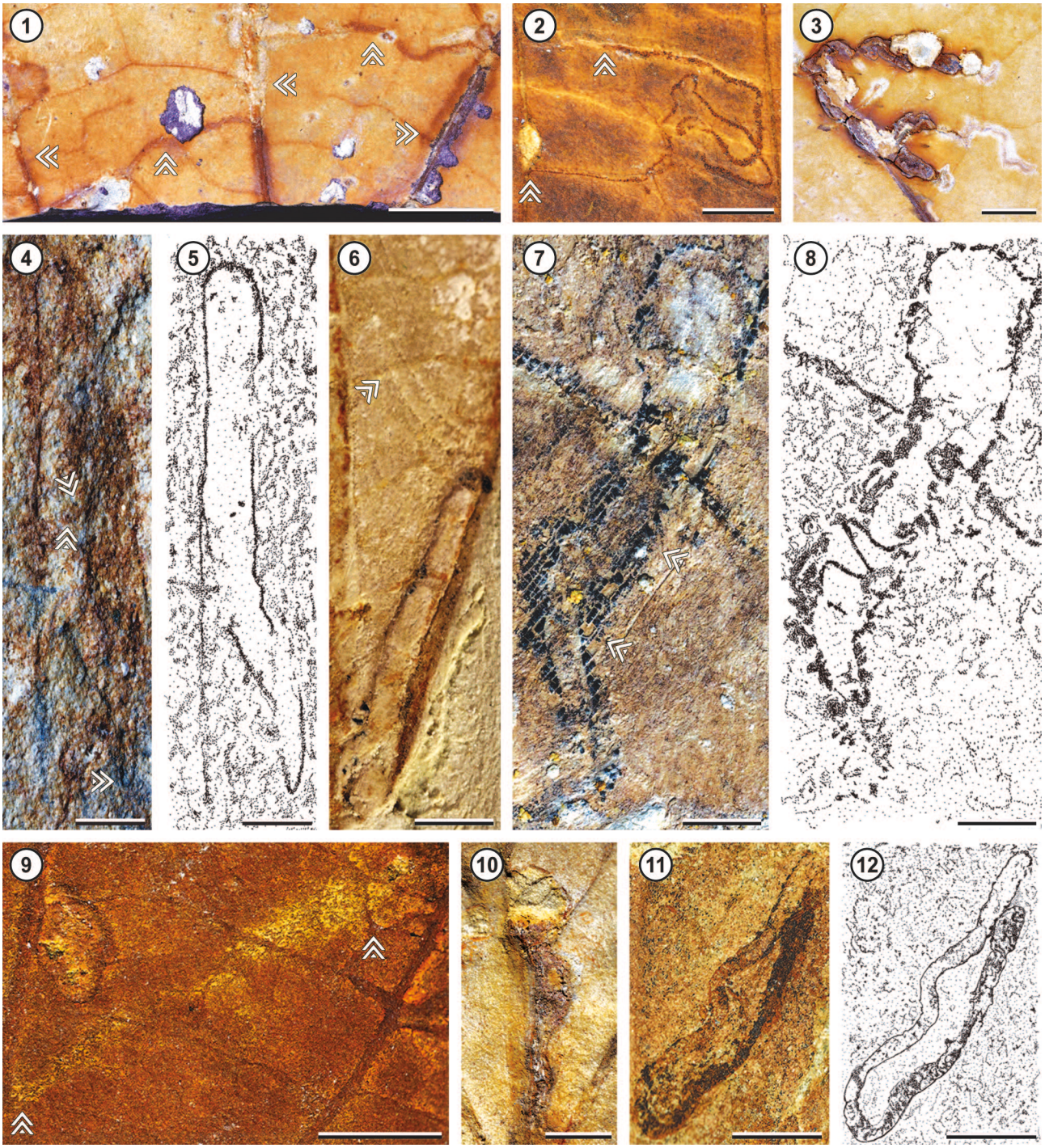

Figure 9. Leaf mining of Paleocene leaves of the Bogotá Formation (Colombia). **1,** Serpentine mine with several 90° turns whose trajectory is determined by secondary and tertiary veins (white arrows; DT105) on leaf morphotype BF4 (Malvaceae; **STRI** 12206). Scale bar equals 5 mm. **2,** Two threadlike serpentine mines (white arrows) confined to areas circumscribed by tertiary veins (DT109) on leaf morphotype BF4 (Malvaceae; **STRI** 47397). Scale bar equals 2 mm. **3,** Mine with occasional width constrictions and a prominent reaction rim, whose trajectory is controlled by primary and secondary veins (DT367) on leaf morphotype BF4 (Malvaceae; **STRI** 12194). Scale bar equals 5 mm. **4,** Curvilinear mine with distinct oviposition site (lower white arrow), dispersed coprolites (upper white arrows) and most of its course running along a secondary vein (DT90) on leaf morphotype BF7 (Lauraceae; **STRI** 46562). Scale bar equals 1 mm. **5, STRI** 46562-DT90 camera-lucida drawing. Scale bar equals 1 mm. **6,** A linear mine with slight width increases and whose last phase runs along the leaf margin (white arrow; DT99) on leaf morphotype BF11 (**STRI** 47354). Scale bar equals 1 mm. **7,** Tortuous broad mine with serpentine deployed frass (white arrows, DT139) on leaf morphotype BF24 (**STRI** 47389). Scale bar equals 2 mm. **8, STRI** 47389-DT139 camera-lucida drawing. Scale bar equals 2 mm. **9,** Linear mine with constant width increases and lack of frass, with a terminal blotch-like phase morphology (rightmost arrow; DT152) on leaf morphotype BF13 (*aff.* Elaeocarpaceae; **STRI** 12014). Scale bar equals 5 mm. **10,** Serpentine mine with an elliptical terminal chamber and seemingly fluidized frass. The mine's trajectory is limited by a primary vein (DT44) on leaf morphotype BF23 (*aff.* Salicaceae; **STRI** 12232). Scale bar equals 2 mm. **11,** Short serpentine mine with one tight 180° degree turn midway through its course (DT177) on leaf morphotype BF38 (Fabaceae; **STRI** 46982). Scale bar equals 2 mm. **12, STRI** 46982-DT177 camera-lucida drawing. Scale bar equals 2 mm.

and 19.3 (± 2.3) are highly specialized DTs (HS = 3); 18.3 (± 1.8) are galling DTs and 7.0 (± 1.8) are leaf mines.

Conservative DT scoring

When using a conservative approach, the number of insect-feeding DTs is reduced to 72. This reduction pertains to the FFGs of piercing-and-sucking, galling and margin feeding, with four, three and one rescored DTs, respectively (see Supplementary Online Information, Supplementary Table 1 on reasoning on DT reinterpretation). With the rescoring, a total of 54.1 (± 3.1) distinct DTs were observed across 400 randomly sampled leaves; 32.2 (± 2.5) being specialized DTs (HS = 2–3), 18.3 (± 2.2) highly specialized DTs (HS = 3) and 15.4 (± 1.8) galling DTs. This still represents an elevated number of DTs (see Supplementary Online Information, Supplementary Figure 1).

DISCUSSION

The vast majority of insect-mediated leaf damage found in the Bogotá flora is related directly to insect herbivory. Of the 86 insect-mediated DTs found in the Bogotá flora, 80 are the result of herbivory-related DTs (six are oviposition lesion DTs) found across 894 non-monocot angiosperms allocated to 48 plant host morphotypes. Only four DTs are attributed to pathogens. The number of herbivory-related DTs exceeds other previously reported and comparable Paleocene flora from North America (Wilf & Labandeira, 1999; Labandeira *et al.*, 2002a, 2002b; Wilf *et al.*, 2006), Europe (Wappler *et al.*, 2009; Wappler & Denk, 2011), Patagonia (Donovan *et al.*, 2016, 2018) or northern South America, namely the Cerrejón flora (Wing *et al.*, 2009). After standardizing for sampling effort, the Bogotá flora continues to have the highest DT richness and DT frequency com-

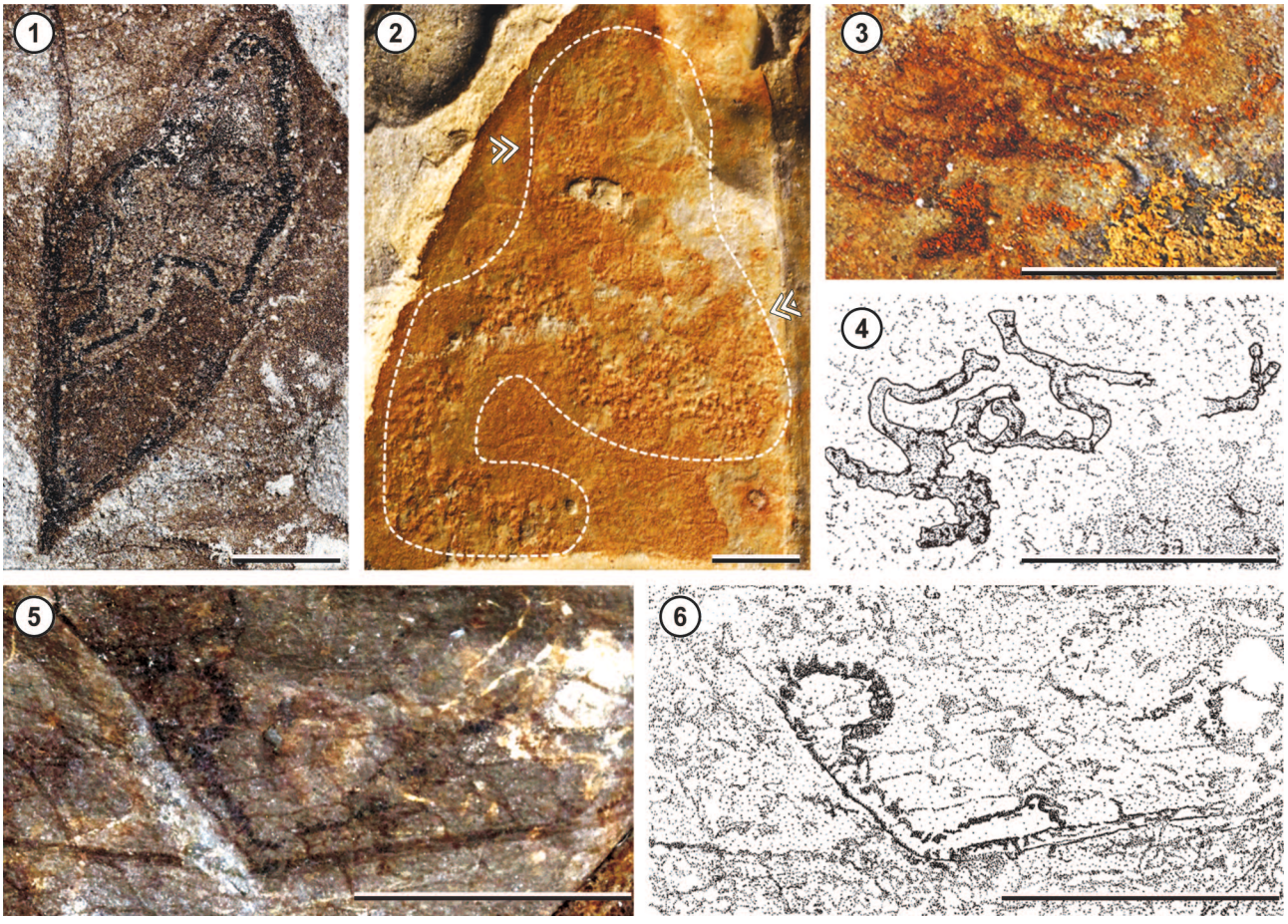

Figure 10. Leaf mining (continued) of Paleocene leaves of the Bogotá Formation (Colombia). **1,** Blotch mine with a tightly packed sinusoidal frass trail (DT37) on leaf morphotype BF41 (**STRI** 12466). Scale bar equals 2 mm. **2,** Short mine with increasing width and transversely deployed frass (dotted line; DT43) on leaf morphotype BF42 (**STRI** 12905). Scale bar equals 2 mm. **3,** A short mine with frequent bifurcations and course reversing (DT207) on leaf morphotype BF42 (**STRI** 47378). Scale bar equals 2 mm. **4, STRI** 47378-DT207 camera-lucida drawing. Scale bar equals 2 mm. **5,** Linear mine controlled by venation, with dark borders and a circular terminal chamber (DT234) on an unidentified leaf morphotype (STRI 12640). Scale bar equals 2 mm. **6, STRI** 12640-DT234 camera-lucida drawing. Scale bar equals 2 mm.

pared to any Paleocene flora (Fig. 11), suggesting that plant-insect herbivore interactions were much more intense at the Bogotá flora than elsewhere during this time period. These differences are also seen when using a more conservative scoring system (see Materials and Methods; Supplementary Online Information, Supplementary Figure 1, Supplementary Table 1), suggesting that the richness of the underlying biological associations is not likely to be an artifact of preservation or DT scoring approach. Given that the number of insect-feeding damage on extant leaves is positively correlated with the richness of the respective unsampled damage makers (Carvalho *et al.*, 2014), the high DT richness recorded for the Bogotá flora most likely reflects a rich array of herbivorous insects, perhaps the richest across comparable Paleocene floras found so far. We note that the Bogotá leaf samples were collected from two localities that are a few meters adjacent to one another, similar in lithology and close stratigraphically. Thus, minimal time-averaging is expected, validating comparisons with North American and Patagonian floras that represent single time slices.

Both the Bogotá and Cerrejón floras resemble modern Neotropical rainforests—in terms of paleoclimate, physiognomy, and floristics—but their plant-insect interactions contrast remarkably. Across 400 randomly sampled leaves, insect feeding damage is abundant at Cerrejón (50.1%), but DT richness is low (24.4 DTs) (Wing *et al.*, 2009), whereas at Bogotá, leaves are much more frequently damaged (69.5%) and bear 2.5 times as many DTs (61.0 DTs) as those of the Cerrejón flora (Fig. 11.1, 11.4). Similar differences in DT richness are seen when using a conservative scoring approach that considers biases in the preservation of detailed structures associated with galling and piercing-and-sucking DTs attributable to taphonomy (see Materials and Methods; Supplementary Online Information, Supplementary Figure 1.1, 1.4).

Most damage in the Cerrejón flora is generalized external feeding (Wing *et al.*, 2009). In contrast, the Bogotá flora has abundant specialized interactions, particularly mines and galls (see below), consistent with the typical host-specialized feeding associations seen in modern Neotropical rainforests (Dyer *et al.*, 2007). The low DT diversity at Cerrejón had been hypothesized to reflect a slow recovery of the Neotropical biota after the end-Cretaceous extinction and/or ecosystems in an early diversification stage (Wing *et al.*, 2009). The contrastingly higher DT richness of total and specialized herbivore associations in the Bogotá flora suggests differences in recovery from the end-Cretaceous event, and a notable ecological heterogeneity among early Neotropical rainforests in northern South America.

Even though both the coeval Bogotá and Cerrejón floras represent Neotropical rainforest environments, they differ in precipitation and depositional environment. Whereas the forests of Bogotá had an annual rainfall of 182–184 cm yr^{-1} and prevailed in well-drained, highly oxidized soils (Morón *et al.*, 2013), the forests of Cerrejón inhabited a regime of higher rainfall (~324 cm yr^{-1}) and grew in saturated soils with little to no oxidation. Estimates of species leaf mass per area (**LMA**) are overall higher and include a wider range of values in the Bogotá than in the Cerrejón flora (Tab. 1; Bogotá: 52–206 g m^{-2} vs. Cerrejón: 44–125 g m^{-2}; see Supplementary Online Information, Supplementary Figure 2 for host-level leaf mass per area estimates). These differences are consistent with the lower, probably seasonal, precipitation seen in Bogotá (Wright *et al.*, 2005) but do not entirely explain the rich and intense feeding damage in this flora. Based on LMA differences alone, the Cerrejón flora is expected to have overall more leaf damage, as rates

TABLE 1. Leaf mass per area (LMA) estimates in Bogotá and Cerrejón floras.

Locality	N	Mean LMA (g/m^2)	95% prediction interval upper limit	95% prediction interval lower limit
Bogotá	13	128.39	144.66	113.95
Cerrejón	15	92.49	102.99	83.05

LMA estimates are based on the method of Royer *et al.* (2007), based on the scaling relationship between petiole width and leaf area. *t*-test indicates that LMA is significantly higher in Bogotá ($P < 0.001$).

of insect herbivory are typically higher on fast-growing trees with short leaf lifespans (Coley *et al.*, 1985) that correlate with low LMA (Wright *et al.*, 2004; Royer *et al.*, 2007; Onoda *et al.*, 2017). It is possible that the wider range of LMA values seen in the Bogotá flora reflects a greater diversity of secondary metabolites and chemical defenses reflect and drive herbivore richness (War *et al.*, 2018).

A defining feature of the Bogotá flora is the high number and frequency of specialized interactions, particularly mines and galls made by host-specialized insects (Powell *et al.*, 1998; Raman *et al.*, 2005). Insects are considered host-specialized if they feed on one or a few closely related plant morphotypes (Labandeira *et al.*, 2007), and specialized DTs more closely map biological species and genera than generalized DTs (Wilf, 2008). For instance, unique mine morphologies within a single plant-host morphotype suggest a single insect culprit species (Donovan *et al.*, 2014). Across 400 randomly sampled leaves, the percentage of leaves with mines in the Bogotá flora (1.8%) is less than other Paleocene localities such as Menat (2.6%) or Mexican Hat (2.6%) in the Northern Hemisphere, but the number of distinct mines is highest (7.0) across comparable floras (Fig. 11.2, 11.5); this is also true for a conservative scoring approach (Supplementary Online Information, Supplementary Figure 1.2, 1.5). A total of 13 mining DTs were found across nine plant hosts in the Bogotá flora. Two leaf morphotypes (BF4 and BF42) had three mining DTs each, one of which is first reported from this flora (DT367 associated with BF4; Fig. 9.3). The high richness of mining DTs on a broad spectrum of host lineages—such as Fabaceae, Malvaceae, Elaeocarpaceae,

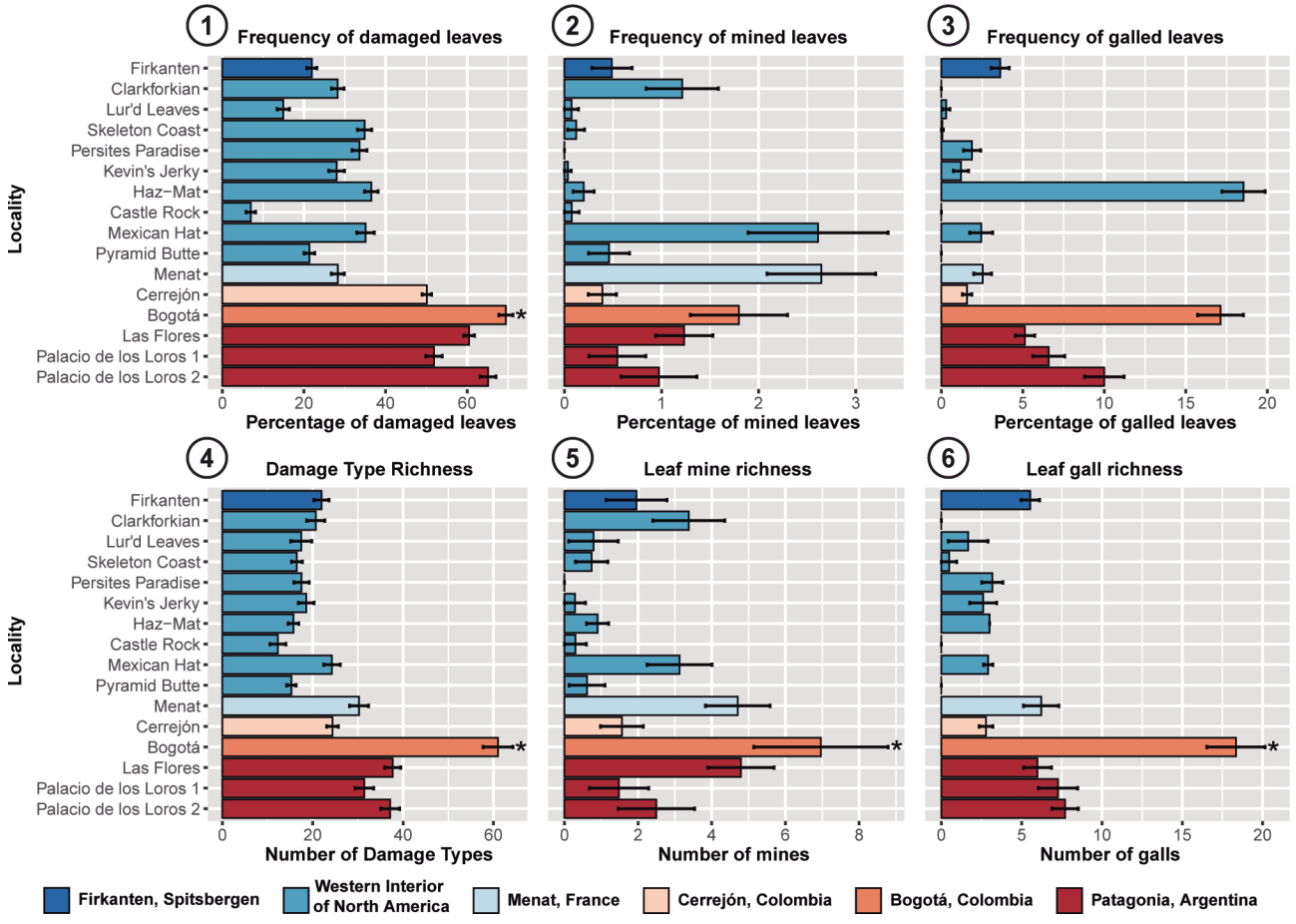

Figure 11. Insect-feeding damage frequency and richness from Paleocene bulk floras of Firkanten, Spitsbergen; Western Interior of North America; Menat, France; Cerrejón, Colombia; Bogotá, Colombia; and Patagonia, Argentina. Percentage of leaves with **1,** total damage; **2,** mines; and **3,** galls. Richness of **4,** total damage; **5,** mines; and **6,** galls. Values are means of 400 leaves, resampled without replacement for 5000 iterations; error bars are ±1*s*. Asterisks indicate cases where the analyzed metric is significantly higher in the Bogotá flora (one-way ANOVA, followed by Tukey HSD test; $P < 0.001$).

Lauraceae, and Salicaceae—suggests that host-specific associations were a common feature at the Bogotá flora. Furthermore, host-specific interactions are also evidenced in the high frequency and richness of galling DTs. Twenty-four gall DTs, 18 of which are specialized (HS = 2–3), were found in the Bogotá flora. The average number of galls (18.3) among 400 leaves is much higher than on any other comparable Paleocene locality, although the frequency (17.1%) of galls is closely surpassed by the Haz-Mat locality (18.5%) from the Western Interior of North America (Fig. 11.3, 11.6); similar patterns are observed with a conservative DT scoring (Supplementary Online Information, Supplementary Figure 1.3, 1.6). The Patagonian Palacio de los Loros 2 flora is second richest in galling DTs, with only 7.7 galls found in 400 leaves (Fig. 11.6).

The high galling DT richness found at the Bogotá flora is ecologically consistent with the high richness of galls found on the canopy of modern tropical rainforests (Julião *et al.*, 2014). In modern ecosystems, the highest diversity of gall-inducing insects is found in xeric environments (Fernandes & Price, 1992; Price *et al.*, 1998), characterized by warm climates, dry and nutrient-poor soils, and low water availability (Price *et al.*, 1998). In tropical rainforests, the intense solar radiation, leaf temperatures approaching lethal limits, and high vapor-pressure deficit experienced in the upper canopy, mimic some of the ambient conditions observed in xeric environments (Julião *et al.*, 2014). As such, the upper canopy of tropical rainforests bears a high galling insect richness (Julião *et al.*, 2014). For instance, in the upper canopy of Amazonian rainforests, the gall richness-to-tree species sampled ratio can be up to 2.5 times higher than the highest value reported for xeric environments (Julião *et al.*, 2014). Although the Cerrejón flora is also a tropical rainforest environment, the lower frequency and richness of leaf galls is consistent with the depositional environments of both floras (see above). The highest abundance and diversity of galling insects among tropical rainforests are found in sites where plants grow in soils of low to moderate nutrient status (Blanche & Westoby, 1995; Gonçalves-Alvim & Fernandes, 2001; Cuevas-Reyes *et al.*, 2003, 2004) or under water limitations (Fernandes & Price, 1988; Waring & Price, 1990). The Bogotá flora experienced lower rainfall than the Cerrejón flora, and potentially lower nutrient availability due to heavily oxidized soils (Vitousek & Sanford, 1986; Fujii *et al.*, 2018), suggesting that the patterns observed in living rainforests may explain the differences in galling richness and frequency observed among Paleocene Neotropical rainforests.

Given that fossil leaf assemblages are overrepresented by canopy leaves (Spicer, 1981; Ferguson, 1985; Smith & Nufio, 2004), questions related to the upper canopy can potentially be addressed in the leaf fossil record. We asked whether the most abundant morphotypes in the Bogotá flora also are frequently damaged by galls and bear a high number of galling DTs: an expected pattern derived from upper canopy leaves of modern tropical rainforests. In accordance with our expectations, the five most common leaf morphotypes—that together account for 45% of all non-monocot angiosperms—have more than 20% of their leaves damaged by galls (Tab. 2) and include 18 of 24 gall DTs observed in the Bogotá flora, and 16 out of 21 galls for the conservative DT scoring approach (Supplementary Online Information, Supplementary Table 2). These five galled leaf morphotypes represent lineages such as Malvaceae,

TABLE 2. Galling damage frequency and richness on abundant morphotypes (>20 leaf specimens). Values at 20 leaves are means of 5000 random resamples of 20 leaves each, without replacement. Indicated uncertainties are ±1*s*.

Morphotype	Leaf specimens	% Leaves with galls	Gall DTs	#Galls at 20 leaves	Taxonomical affinity
BF13	166	21.0 ± 8.6	10	3.3 ± 1.4	Elaeocarpaceae?
BF4	61	21.4 ± 7.5	9	5.1 ± 1.6	Malvaceae
BF12	21	38.1 ± 2.4	8	7.7 ± 0.5	?
BF37	110	23.5 ± 8.6	8	3.4 ± 1.3	Euphorbiaceae
BF36	44	24.8 ± 7.3	7	4.4 ± 1.4	Ulmaceae

Elaeocarpaceae and Euphorbiaceae, and are associated with trees that are likely present in the upper canopy. This observation suggests that the Bogotá flora is similar to modern tropical forests in the preferential use of upper canopy leaves by gall-inducing insects.

The high plant diversity seen in modern Neotropical rainforests might owe, at least in part, to a legacy of rich plant-insect associations during the Paleocene. In modern ecosystems, herbivorous insects promote plant diversity via reduced population growth rates of plants that become locally common (Janzen, 1970; Connell, 1971). This process is one of several mechanisms that underlie negative density-dependence (Forrister *et al.*, 2019) and therefore is hypothesized to contribute to driving and maintaining plant diversity in the tropics (LaManna *et al.*, 2017). While species-specific and more generalized mechanisms can cause negative density-dependence, only host-specific interactions that drive negative density-dependence can maintain diversity (Janzen, 1970; Connell, 1971; Terborgh, 2012). The frequent, rich and host-specialized plant-insect associations of the Bogotá flora suggest a deep historical context for negative density-dependence as a potential driver (and maintainer) of the high plant diversity observed in modern Neotropical rainforests. Leaf herbivory at the Bogotá flora also suggests stronger negative density-dependence mechanisms in the tropics than elsewhere since the late Paleocene.

CONCLUSIONS

The Bogotá flora bears high herbivore pressure, rich and specialized insect-feeding associations, and a preferential use of canopy leaves by gall-inducing insects. All this suggests that some of the main features of insect herbivore ecology of modern Neotropical rainforests are depicted by the Bogotá flora. Given that herbivorous insects promote and maintain plant diversity in the tropics, the high plant diversity observed in modern Neotropical rainforests might owe—at least in part—to the legacy of rich plant-insect herbivore associations of the Paleocene.

ACKNOWLEDGMENTS

The authors thank Arcillas de Colombia and Cantera Tablegares for permission to work in their mines; E. Cadena for providing constructive comments on the manuscript; M. Donovan and P. Wilf for providing the Western Interior of North America herbivory data; A. Alfonso and L. Oviedo for assistance with fieldwork; J. Betancur, A. Cespedes, A. Pérez, W. Echavarría and K. Cárdenas for laboratory assistance; D. Carvalho for photographing assistance; and the Instituto de Investigaciones en Estratigrafía at Universidad de Caldas for providing access to research facilities. A. Giraldo thanks A. Cárdenas for the constant support, as well as the STRI Short Term Fellowship program. This research was funded by NSF Grant EAR-1829299 to M. Carvalho and F. Herrera; Earl S. Tupper Postdoctoral Fellowship to M. Carvalho; and the Oak Spring Garden Foundation to F. Herrera. This is contribution 396 of the Evolution of Terrestrial Ecosystems consortium at the National Museum of Natural History, in Washington, D.C.

REFERENCES

Bairstow, K. A., Clarke, K. L., McGeoch, M. A., & Andrew, N. R. (2010). Leaf miner and plant galler species richness on Acacia: Relative importance of plant traits and climate. *Oecologia*, *163*(2), 437–448.

Bayona, G., Cortés, M., Jaramillo, C., Ojeda, G., Aristizabal, J. J., & Reyes-Harker, A. (2008). An integrated analysis of an orogen-sedimentary basin pair: Latest Cretaceous-Cenozoic evolution of the linked Eastern Cordillera orogen and the Llanos foreland basin of Colombia. *Bulletin of the Geological Society of America*, *120*(9–10), 1171–1197.

Bayona, G., Montenegro, O., Cardona, A., Jaramillo, C. A., Lamus, F., Morón, S., Quiroz, L., Ruiz, M., Valencia, V., Parra, M., & Stockli, D. (2010). Estratigrafía, procedencia, subsidencia y exhumación de las unidades Paleógenas en el Sinclinal de Usme, sur de la zona axial de la Cordillera Oriental. *Geología Colombiana*, *35*, 5–35.

Blanche, K. R., & Westoby, M. 1995. Gall-forming insect diversity is linked to soil fertility via host plant taxon. *Ecology*, *76*(7), 2334–2337.

Bloch, J. I., Cadena, E., Hastings, A., Rincon, A. F., & Jaramillo, C. (2008). Vertebrate faunas from the Paleocene Bogotá Formation of Northern Colombia. *Journal of Vertebrate Paleontology*, *3*, 53–53.

Burnham, R. J., & Johnson, K. R. (2004). South American palaeobotany and the origins of neotropical rainforests. *Philosophical Transactions of the Royal Society B: Biological Sciences*, *359*(1450), 1595–1610.

Cadena, E. A. (2014). The fossil record of turtles in Colombia: a review of the discoveries, research and future challenges. *Acta Biológica Colombiana*, *19*(3), 333–339.

Carvalho, M., Wilf, P., Barrios, H., Windsor, D. M., Currano, E. D., Labandeira, C. C., & Jaramillo, C. A. (2014). Insect Leaf-Chewing Damage Tracks Herbivore Richness in Modern and Ancient Forests. *PLoS ONE*, *9*(5), Article e94950. https://doi.org/10.1371/journal.pone.0094950

Coley, P. D., & Aide, T. M. (1991). Comparison of herbivory and plant defenses in temperate and tropical broad-leaved forests. In P. W. Price, T. M. Lewinsohn, G. W. Fernandes, & B. B. Benson (Eds.), *Plant animal interactions: evolutionary ecology in tropical and temperate regions* (pp. 25–49). Wiley.

Coley, P. D., Bryant, J. P., & Chapin, S. (1985). Resource availability and plant antiherbivore defense. *Science*, *230*(4728), 895–899. https://doi.org/10.1126/science.230.4728.895

Connell, J. H. (1971). On the role of natural enemies in preventing competitive exclusion in some marine animals and in rain forest trees. In P. J. Den Boer & G. Gradwell (Eds.), *Dynamics of populations* (pp. 298–312). Center for Agricultural Publishing and Documentation.

Crespi, B. J., Carmean, D. A., & Chapman, T. W. (1997). Ecology and evolution of galling thrips and their allies. *Annual Review of Entomology*, *42*(1), 51–71.

Cuevas-Reyes, P., Quesada, M., Siebe, C., & Oyama, K. (2004). Spatial patterns of herbivory by gall-forming insects: A test of the soil fertility hypothesis in a Mexican tropical dry forest. *Oikos*, *107*(1), 181–189.

Cuevas-Reyes, P., Siebe, C., Martinez-Ramos, M., & Oyama, K. (2003). Species richness of gall-forming insects in a tropical rain forest: correlations with plant diversity and soil. *Biodiversity and Conservation*, *1*(12), 411–422.

Donovan, M. P., Iglesias, A., Wilf, P., Labandeira, C. C., & Cúneo, N. R. (2016). Rapid recovery of Patagonian plant-insect associations after the end-Cretaceous extinction. *Nature Ecology and Evolution*, *1*(12), 1–5.

Donovan, M. P., Iglesias, A., Wilf, P., Labandeira, C. C., & Cúneo, N. R. (2018). Diverse Plant-Insect Associations from the Latest Cretaceous and Early Paleocene of Patagonia, Argentina. *Ameghiniana*, *55*(3), 303–338.

Donovan, M. P., Wilf, P., Labandeira, C. C., Johnson, K. R., & Peppe, D. J. (2014). Novel insect leaf-mining after the end-Cretaceous extinction and the demise of Cretaceous leaf miners, Great Plains, USA. *PLoS ONE*, *9*(7), Article e103542. https://doi.org/10.1371/journal.pone. 0103542

Dyer, L. A., Singer, M. S., Lill, J. T., Stireman, J. O., Gentry, G. L., Marquis, R. J., Ricklefs, R. E., Greeney, H. F., Wagner, D. L., Morais, H. C., Diniz, I. R., Kursar, T. A., & Coley, P. D. (2007). Host specificity of Lepidoptera in tropical and temperate forests. *Nature*, *448*(7154), 696–699.

Ellis, B., Daly, D. C., Hickey, L. J., Mitchell, J. D., Johnson, K. R., Wilf, P., & Wing, S. L. (2009). *Manual of Leaf Architecture*. Cornell University Press; New York Botanical Garden.

Ferguson, D. K. (1985). The origin of leaf-assemblages – new light on an old problem. *Review of Palaeobotany and Palynology*, *46*(1–2), 117–188.

Fernandes, G. W., & Price, P. W. (1988). Biogeographical gradients in galling species richness: tests of hypotheses. *Oecologia*, *76*(1), 161–167.

Fernandes, G. W., & Price, P. W. (1992). The adaptive significance of insect gall distribution: survivorship of species in xeric and mesic habitats. *Oecologia*, *90*(1), 14–20.

Forrister, D. L., Endara, M.-J., Younkin, G. C., Coley, P. D., & Kursar, T. A. (2019). Herbivores as drivers of negative density dependence in tropical forest saplings. *Science*, *363*(6432), 1213–1216.

Fujii, K., Shibata, M., Kitajima, K., Ichie, T., Kitayama, K., & Turner, B. L. (2018). Plant–soil interactions maintain biodiversity and functions of tropical forest ecosystems. *Ecological Research*, *33*(1), 149–160. https://doi.org/10.1007/s11284-017-1511-y

Gonçalves-Alvim, S. J., & Fernandes, G. W. (2001). Biodiversity of galling insects : Historical , community and habitat effects in four neotropical savannas Biodiversity of galling insects : historical, community and habitat effects in four neotropical savannas. *Biodiversity and Conservation*, *10*(1), 79–98.

Graham, H. V., Herrera, F., Jaramillo, C., Wing, S. L., & Freeman, K. H. (2019). Canopy structure in Late Cretaceous and Paleocene forests as reconstructed from carbon isotope analyses of fossil leaves. *Geology*, *47*(10), 977–981.

Head, J. J., Bloch, J. I., Rincón, A., Moreno-Bernal, J. W., & Jaramillo, C. (2012). Paleogene squamates from the northern neotropics: ecological implications and biogeographic histories. *Journal of Vertebrate Paleontology*, *32*(2), 108.

Herrera, F., Carvalho, M. R., Wing, S. L., Jaramillo, C., & Herendeen, P. S. (2019). Middle to late Paleocene leguminosae fruits and leaves from Colombia. *Australian Systematic Botany*, *32*(6), 385–408.

Herrera, F., Manchester, S. R., Carvalho, M. R., Jaramillo, C., & Wing, S. L. (2014). Paleocene wind-dispersed fruits and seeds from Colombia and their implications for early Neotropical rainforests. *Acta Palaeobotanica*, *54*(2), 197–229.

Herrera, F., Manchester, S. R., Hoot, S. B., Wefferling, K., Carvalho, M. R., & Jaramillo, C. (2011). Phytogeographic implications of fossil endocarps of Menispermaceae from the Paleocene of Colombia. *American Journal of Botany*, *8*(12), 2004–2017.

Janzen, D. H. (1970). Herbivores and the Number of Tree Species in Tropical Forests. *The American Naturalist*, *104*(940), 501–528.

Jaramillo, C. (2020). *Smithsonian Tropical Research Institute Geological Sample Database*. https://biogeodb.stri.si.edu/jaramillosdb/web/fossils/

Jaramillo, C. A., Bayona, G., Harrington, G. J., Pardo-Trujillo, A., Mora, G., Rueda, M., & Torres, V. (2007). The Palynology of the Cerrejón Formation (Upper Paleocene) of Northern Colombia. *Palynology*, *31*(1), 153–189.

Jaramillo, C. A., Rueda, M., & Torres, V. (2011). A palynological zonation for the Cenozoic of the Llanos and Llanos Foothills of Colombia. *Palynology*, *35*(1), 46–84.

Julião, G. R., Venticinque, E. M., Fernandes, G. W., & Price, P. W. (2014). Unexpected high diversity of galling insects in the Amazonian upper canopy: The savanna out there. *PLoS ONE*, *9*(12), Article e114986. https://doi.org/10.1371/journal.pone.0114986

Labandeira, C. C. (2019). The fossil record of insect mouthparts: Innovation, functional convergence and associations with other organisms. *Zoological Monographs*, *5*, 567–671.

Labandeira, C. C., Johnson, K. R., & Lang, P. (2002a). Preliminary assessment of insect herbivory across the Cretaceous-Tertiary boundary: Major extinction and minimum rebound. *Geological Society of America Special Paper*, *361*, 297–327.

Labandeira, C. C., Johnson, K. R., & Wilf, P. (2002b). Impact of the terminal Cretaceous event on plant – insect associations. *Proceedings of the National Academy of Sciences*, *99*(4), 2061–2066.

Labandeira, C. C., & Prevec, R. (2014). Plant paleopathology and the roles of pathogens and insects. *International Journal of Paleopathology*, *4*(1), 1–16.

Labandeira, C. C., Wilf, P., Johnson, K. R., & Marsh, F. (2007). *Guide to Insect (and Other) Damage Types on Compressed Plant Fossils*. Version 3.0. Smithsonian Institution.

LaManna, J. A., Mangan, S. A., Alonso, A., Bourg, N. A., Brockelman, W. Y., Bunyavejchewin, S., Chang, L. W., Chiang, J. M., Chuyong, G. B., Clay, K., Condit, R., Cordell, S., Davies, S. J., Furniss, T. J., Giardina, C. P., Gunatilleke, I. A. U. N., Gunatilleke, C. V. S., He, F., Howe, R. W., … Myers, J. A. (2017). Plant diversity increases with the strength of negative density dependence at the global scale. *Science, 356*(6391), 1389–1392. https://doi.org/10.1126/science.aam5678

Morón, S., Fox, D. L., Feinberg, J. M., Jaramillo, C., Bayona, G., Montes, C., & Bloch, J. I. (2013). Climate change during the Early Paleogene in the Bogotá Basin (Colombia) inferred from paleosol carbon isotope stratigraphy, major oxides, and environmental magnetism. *Palaeogeography, Palaeoclimatology, Palaeoecology*, *388*, 115–127.

Novotny, V., Drozd, P., Miller, S. E., Kulfan, M., Janda, M., Basset, Y., & Weiblen, G. D. (2006). Why are there so many species of herbivorous insects in tropical rainforests? *Science*, *313*(5790), 1115–1118.

Novotny, V., Miller, S. E., Hulcr, J., Drew, R. A. I., Basset, Y., Janda, M., Setliff, G. P., Darrow, K., Stewart, A. J. A., Auga, J., Isua, B., Molem, K., Manumbor, M., Tamtiai, E., Mogia, M., & Weiblen, G. D. (2007). Low beta diversity of herbivorous insects in tropical forests. *Nature*, *448*(7154), 692–695.

Onoda, Y., Wright, I. J., Evans, J. R., Hikosaka, K., Kitajima, K., Niinemets, Ü., Poorter, H., Tosens, T., & Westoby, M. (2017).

Physiological and structural tradeoffs underlying the leaf economics spectrum. *New Phytologist*, *214*(4), 1447–1463. https://doi.org/10.1111/nph.14496

Powell, J. A., Mitter, C., & Farrell, B. D. (1998). Evolution of larval food preferences in Lepidoptera. In N. P. Kristensen (Ed.), *Handbook of Zoology: Vol. 4. Arthropoda: Insecta, Part 35. Lepidoptera, Moths and Butterflies* (pp. 403–422). W. de Gruyter.

Price, P. W., Fernandes, G. W., Lara, A. C. F., Brawn, J., Barrios, H., Wright, M. G., Ribiero, S. P., & Rothcliff, N. (1998). Global patterns in local number of insect galling species. *Journal of Biogeography*, *25*, 581–591.

R Core Team. (2020). *R: A Language and Environment for Statistical Computing*. Version 4.0. R Foundation for Statistical Computing. https://www.R-project.org

Raman, A., Schaefer, C. W., & Withers, T. M. (2005). Biology, Ecology, and Evolution of Gall-Inducing Arthropods. In A. Raman, C. W. Schaefer, & T. M. Withers (Eds.), *Biology, Ecology, and Evolution of Gall-Inducing Arthropods* (pp. 1–33). Taylor & Francis.

Royer, D., Sack, L., Wilf, P., Lusk, C. H., Jordan, G. J., Niinemets, Ü., Wright, I. J., Westoby, M., Cariglino, B., Coley, P. D., Cutter, A. D., Johnson, K. R., Labandeira, C. C., Moles, A. T., Palmer, M. B., & Valladares, F. (2007). Fossil leaf economics quantified: calibration, Eocene case study, and implications. *Paleobiology*, *33*(4), 574–589.

Schneider, C. A., Rasband, W. S., & Eliceiri, K. W. (2012). NIH Image to ImageJ: 25 years of image analysis. *Nature Methods*, *9*(7), 671–675.

Smith, D. M. , & Nufio, C. R. (2004). Levels of Herbivory in Two Costa Rican Rain Forests: Implications for Studies of Fossil Herbivory. *Biotropica*, *36*(3), 318–326.

Spicer, R. A. (1981). The sorting and deposition of allochthonous plant material in a modern environment at Silwood Lake, Silwood Park, Berkshire, England. *US Geological Survey, Professional Paper*, Article 1143. https://doi.org/10.3133/pp1143

Stull, G. W., Herrera, F., Manchester, S. R., Jaramillo, C., & Bruce, H. (2012). Fruits of an "Old World" tribe (Phytocreneae; Icacinaceae) from the Paleogene of North and South America. *Systematic Botany*, *37*(3), 784–794.

Terborgh, J. (2012). Enemies maintain hyperdiverse tropical forests. *American Naturalist*, *179*(3), 303–314.

Villaroel, A. C. (1987). Características y afinidades de *Etayoa* n. gen., tipo de una nueva familia de Xenungulata (Mammalia) del Paleoceno medio (?) de Colombia. *Comunicaciones paleontológicas del Museo de Historia Natural de Montevideo*, *19*, 241–253.

Vitousek, P. M., & Sanford, R. L. (1986). Nutrient cycling in moist tropical forest. *Annual Review of Ecology and Systematics*, *17*, 137–167. https://doi.org/10.1146/annurev.es.17.110186.001033

Wappler, T., Currano, E. D., Wilf, P., Rust, J., & Labandeira, C. C. (2009). No post-Cretaceous ecosystem depression in European forests? Rich insect-feeding damage on diverse middle Palaeocene plants, Menat, France. *Proceedings of the Royal Society B: Biological Sciences*, *276*(1677), 4271–4277.

Wappler, T., & Denk, T. (2011). Herbivory in early Tertiary Arctic forests. *Palaeogeography, Palaeoclimatology, Palaeoecology*, *310*(3–4), 283–295. https://doi.org/10.1016/j.palaeo.2011.07.020

War, A. R., Taggar, G. K., Hussain, B., Taggar, M. S., Nair, R. M., & Sharma, H. C. (2018). Plant defence against herbivory and insect adaptations. *AoB PLANTS*, *10*(4), Article ply037. https://doi.org/10.1093/aobpla/ply037

Waring, G. L., & Price, P. W. (1990). Plant water stress and gall formation (Cecidomyiidae: *Asphondylia* spp.) on creosote bush. *Ecological Entomology*, *15*(1), 87–95.

Wilf, P. (2008). Insect-damaged fossil leaves record food web response to ancient climate change and extinction. *New Phytologist*, *178*(3), 486–502.

Wilf, P., & Labandeira, C. C. (1999). Response of Plant-Insect Associations to Paleocene-Eocene Warming. *Science*, *284*(5423), 2153–2156.

Wilf, P., Labandeira, C. C., Johnson, K. R., & Ellis, B. (2006). Decoupled Plant and Insect Diversity After the end-Cretaceous Extinction. *Science*, *313*(5790), 1112–1115. https://doi.org/10.1126/science. 1129569

Wing, S. L., Herrera, F., Jaramillo, C. A., Gomez-Navarro, C., Wilf, P., & Labandeira, C. C. (2009). Late Paleocene fossils from the Cerrejón Formation, Colombia, are the earliest record of Neotropical rainforest. *Proceedings of the National Academy of Sciences*, *106*(44), 18627–18632.

Wright, I. J., Reich, P. B., Cornelissen, J. H. C., Falster, D. S., Groom, P. K., Hikosaka, K., Lee, W., Lusk, C. H., Niinemets, Ü., Oleksyn, J., Osada, N., Poorter, H., Warton, D. I., & Westoby, M. (2005). Modulation of leaf economic traits and trait relationships by climate. *Global Ecology and Biogeography*, *14*(5), 411–421. https://doi.org/10.1111/j.1466-822x.2005.00172.x

Wright, I. J., Reich, P. B., Westoby, M., Ackerly, D. D., Baruch, Z., Bongers, F., Cavender-Bares, J., Chapin, T., Cornellssen, J. H. C., Diemer, M., Flexas, J., Garnier, E., Groom, P. K., Gulias, J., Hikosaka, K., Lamont, B. B., Lee, T., Lee, W., Lusk, C., ... Villar, R. (2004). The worldwide leaf economics spectrum. *Nature*, *428*(6985), 821–827. https://doi.org/10.1038/nature02403

doi: 10.5710/AMGH.17.02.2021.3390

Submitted: August 26th, 2020
Accepted: February 17th, 2021
Published: April 30th, 2021